Quantitative mapping of cerebrovascular reactivity amplitude and delay with breath-hold BOLD fMRI when end-tidal CO_2 quality is low

Rebecca G. Clements[1,2], Kristina M. Zvolanek[1,2], Neha A. Reddy[1,2], Kimberly J. Hemmerling[1,2], Roza G. Bayrak[3], Catie Chang[3,4,5], Molly G. Bright[1,2]

[1]Department of Physical Therapy and Human Movement Sciences, Feinberg School of Medicine, Northwestern University, Chicago, IL, USA

[2]Department of Biomedical Engineering, McCormick School of Engineering and Applied Sciences, Northwestern University, Evanston, IL, USA

[3]Department of Electrical and Computer Engineering, Vanderbilt University, Nashville, TN, USA

[4]Department of Biomedical Engineering, Vanderbilt University, Nashville, TN, USA

[5]Department of Computer Science, Vanderbilt University, Nashville, TN, USA

Corresponding Author:

Rebecca G. Clements

645 N. Michigan Ave, Suite 1100

Chicago, IL 60611

USA

t: (856) 656-5100

e: rebecca.clements@northwestern.edu

Keywords: BOLD fMRI, cerebrovascular reactivity, breath-hold task, CO_2, respiration volume per time, deep learning

Abstract

Cerebrovascular reactivity (CVR), the ability of cerebral blood vessels to dilate or constrict in order to regulate blood flow, is a clinically useful measure of cerebrovascular health. CVR is often measured using a breath-hold task to modulate blood CO_2 levels during an fMRI scan. Measuring end-tidal CO_2 ($P_{ET}CO_2$) with a nasal cannula during the task allows CVR amplitude to be calculated in standard units (vascular response per unit change in CO_2, or %BOLD/mmHg) and CVR delay to be calculated in seconds. The use of standard units allows for normative CVR ranges to be established and for CVR comparisons to be made across subjects and scan sessions. Although breath-holding can be successfully performed by diverse patient populations, obtaining accurate $P_{ET}CO_2$ measurements requires additional task compliance; specifically, participants must breathe exclusively through their nose and exhale immediately before and after each breath hold. Meeting these requirements is challenging, even in healthy participants, and this has limited the translational potential of breath-hold fMRI for CVR mapping. Previous work has focused on using alternative regressors such as respiration volume per time (RVT), derived from respiratory belt measurements, to map CVR. Because measuring RVT does not require additional task compliance from participants, it is a more feasible measure than $P_{ET}CO_2$. However, using RVT does not produce CVR in standard units. In this work, we explored how to achieve CVR maps, in standard units, when breath-hold task $P_{ET}CO_2$ data quality is low. First, we evaluated whether RVT could be scaled to units of mmHg using a subset of $P_{ET}CO_2$ data of sufficiently high quality. Second, we explored whether a $P_{ET}CO_2$ timeseries predicted from RVT using deep learning allows for more accurate CVR measurements. Using a dense-mapping breath-hold fMRI dataset, we showed that both rescaled RVT and rescaled, predicted $P_{ET}CO_2$ can be used to produce maps of CVR amplitude and delay in standard units with strong absolute agreement to ground-truth maps. However, the rescaled, predicted $P_{ET}CO_2$ regressor resulted in superior accuracy for both CVR amplitude and delay. In an individual with regions of increased CVR delay due to Moyamoya disease, the predicted $P_{ET}CO_2$ regressor also provided greater sensitivity to pathology than RVT. Ultimately, this work will increase the clinical applicability of CVR in populations exhibiting decreased task compliance.

1. Introduction

Maintaining appropriate cerebral blood flow is critical for supplying a sufficient stream of oxygen and nutrients to the brain. Cerebrovascular reactivity (CVR) reflects the ability of blood vessels in the brain to dilate or constrict in order to regulate blood flow. CVR is typically measured using the dynamic response to a vasodilatory challenge and is complementary to steady-state measures like cerebral blood flow and cerebral blood volume (Liu et al., 2019). CVR has demonstrated clinical utility for a range of conditions including stroke (Papassin et al., 2021), carotid stenosis (Sobczyk et al., 2020), traumatic brain injury (Mathieu et al., 2020), Alzheimer's disease (Yezhuvath et al., 2012), and multiple sclerosis (Chiarelli et al., 2022). CVR is also sensitive to healthy aging (Peng et al., 2018), cognitive function (D. Kim et al., 2021), and exercise (Murrell et al., 2013). In addition to being an important measure of vascular function, CVR has demonstrated potential for calibrating functional magnetic resonance imaging (fMRI) data in order to more confidently assess changes in neural activity (Davis et al., 1998; Liu et al., 2013).

To map CVR in the brain, an fMRI scan is often used; this scan utilizes the blood-oxygenation level-dependent (BOLD) signal to detect changes in cerebral blood flow. Typically, during the scan, arterial CO_2 levels are deliberately increased to induce systemic vasodilation and thus increase blood flow. End-tidal CO_2 ($P_{ET}CO_2$) values, which act as a surrogate for arterial CO_2, are then used to compute CVR in standard units (%BOLD/mmHg). One common approach for increasing arterial CO_2 involves intermittently inhaling air with a fixed concentration of CO_2 (Lu et al., 2014). Computerized approaches have also been developed to dynamically change the inspired gas partial pressures to allow for precise targeting of $P_{ET}CO_2$ (Slessarev et al., 2007; Wise et al., 2007). While these gas delivery approaches allow for robust, reliable CVR characterization (Leung et al., 2016; Sobczyk et al., 2021), they require equipment that is often expensive, time-consuming to set up, and uncomfortable for participants. One highly feasible alternative involves using resting-state fMRI to map CVR by exploiting natural variations in arterial CO_2 due to changes in breathing rate and depth (Golestani et al., 2016; Liu et al., 2017). However, a limitation of this approach is that spontaneous breathing changes may not cause sufficient BOLD signal variation to reliably assess CVR (Pinto et al., 2021). This is supported by De Vis et al. (2018), who found that a hypercapnia stimulus of at least 2 mmHg above baseline $P_{ET}CO_2$ is necessary to effectively evaluate hemodynamic impairment in a group of participants with internal carotid artery occlusive disease.

Completing breath holds during the fMRI scan is a promising method for robustly mapping CVR by invoking large changes in arterial CO_2 levels without external gas delivery (Bright & Murphy, 2013; Kastrup et al., 2001). In addition to requiring less equipment than gas delivery methods, breath holds can also increase participant comfort since they do not require the participant to wear a face mask within the head coil and can be stopped by the participant at any time (Bright & Murphy, 2013). Rather than a face mask, participants typically wear a nasal cannula during the scan so that $P_{ET}CO_2$ can be measured to approximate arterial CO_2 and calculate CVR. Compared to the face mask, participants often report the nasal cannula to be more comfortable due to its minimal contact with the face, breathability, and smaller size, allowing for a better fit within the head coil.

When measuring CVR, and particularly when characterizing a transient or dynamic response such as the response to a breath hold, it is important to consider both the amplitude and timing of the blood flow response. Variations in CVR timing can arise from regional heterogeneities in arterial transit times and variations in local vasodilatory response dynamics (Stickland et al., 2021). One approach for modeling CVR that accounts for both the amplitude and delay of the response at each voxel is a lagged general linear model framework (Moia et al., 2020a; Stickland et al., 2021). In this framework, multiple shifted variants of the $P_{ET}CO_2$ regressor are used to model the BOLD response to the $P_{ET}CO_2$ regressor at each voxel. The shift that maximizes the full model R^2 is used to calculate the CVR amplitude and is considered the hemodynamic delay. Accounting for hemodynamic delays not only improves the accuracy of CVR amplitude estimates, but also provides a complementary measure of cerebrovascular health (Donahue et al., 2015; Stickland et al., 2021). Additionally, since this approach utilizes a $P_{ET}CO_2$ regressor recorded during the scan, CVR amplitude and delay can be calculated in standard units (%BOLD/mmHg and seconds, respectively).

The use of standard units allows normative CVR ranges to be established and CVR comparisons to be made across subjects and scan sessions. However, one challenge with this approach is obtaining accurate $P_{ET}CO_2$ measurements, particularly during breath-hold protocols. There are two main requirements that participants must meet for the recorded $P_{ET}CO_2$ values to accurately approximate arterial CO_2 changes associated with the breath-hold task. First, participants must exhale immediately before and after each breath hold (Bright & Murphy, 2013; Murphy et al., 2011). This is necessary because true end-tidal gas values are only achieved at the end of expirations. However, exhaling before a breath hold may make the breath hold more challenging (although the duration of the breath hold can be shortened accordingly) and exhaling at the end of a breath hold must override and slightly delay the

instinctive urge to take recovery breaths. Second, because $P_{ET}CO_2$ is typically measured using a nasal cannula, participants must breathe through their nose for the entire experiment. If the participant fails to meet these two requirements, the $P_{ET}CO_2$ regressor will have missing data and will otherwise be an inaccurate approximation of arterial CO_2, which will likely result in an inaccurate CVR estimate. Collectively these requirements raise concerns about breath-hold CVR accuracy in pediatric populations and clinical populations such as those with dementia, in which fMRI task compliance is often lower. In fact, a recent study which used a breathing task to map CVR in a pediatric cohort observed age-related differences in task compliance within the cohort, with younger participants having less reliable $P_{ET}CO_2$ values (Stickland et al., 2021).

Respiration volume per time (RVT) is an alternative metric to $P_{ET}CO_2$, which captures changes in breathing rate and depth that likely drive the majority of changes in arterial CO_2 during voluntary breathing modulations (Birn et al., 2006). During task-free resting-state breathing, temporal fluctuations in RVT have been found to be highly correlated with $P_{ET}CO_2$ and to explain similar spatial and temporal BOLD signal variance (Chang & Glover, 2009). RVT can be measured by recording changes in respiration effort using a pneumatic belt worn around the chest or abdomen. Because RVT does not require the participant to exhale before and after each breath hold nor to breathe through their nose, it is often easier to obtain a high-quality and complete RVT trace than a $P_{ET}CO_2$ trace. Additionally, since respiration belts are commonly included with many scanner set-ups (Zvolanek et al., 2023) and relatively comfortable to wear, recording RVT is immediately feasible for most settings and participants, including pediatric and clinical populations.

Previously, Zvolanek et al. (2023) found that when $P_{ET}CO_2$ data quality is sufficient, RVT can produce CVR amplitude and delay maps that are comparable to those from $P_{ET}CO_2$. The authors defined “sufficient” data as having greater than 50% power in the dominant frequency range of the breath-hold task. Furthermore, they found that when sufficient $P_{ET}CO_2$ recordings are not available, RVT can recover CVR amplitude and delay maps, as long as the participant attempted the breath-hold task (Zvolanek et al., 2023). However, because RVT is measured in arbitrary units, they noted that one limitation of this approach is that the CVR amplitude maps generated using RVT are not in the standard CVR units of %BOLD/mmHg. This means that the CVR amplitude maps can only be used to make relative comparisons between brain regions of a single subject from a single scan and cannot be appropriately compared across subjects or scan sessions.

An alternative approach is using respiration-belt recordings to predict $P_{ET}CO_2$ and then mapping CVR using the predicted $P_{ET}CO_2$ timeseries. This approach may better model the BOLD response to changes in arterial CO_2 compared to using RVT alone. Agrawal et al. (2023) demonstrated the feasibility of predicting the complete CO_2 pressure timeseries from respiration-belt recordings in resting-state data using deep learning. Their predicted CO_2 pressure timeseries achieved a Pearson correlation of 0.946 ± 0.056 with the ground truth CO_2; they also derived $P_{ET}CO_2$ from the predicted CO_2 timeseries and achieved a correlation of 0.512 ± 0.269 with the ground truth. The authors noted that they tried to predict $P_{ET}CO_2$ directly from RVT, but their model performed poorly. Similar to Zvolanek et al. (2023), the authors noted that since RVT is recorded in arbitrary units, they could only predict z-normalized $P_{ET}CO_2$ (0 mean and a standard deviation of 1). Furthermore, the authors exclusively trained and validated their model using resting-state data, and did not extend to breath-hold data.

The goal of the current study is to develop a strategy for mapping CVR amplitude in *standard units* (%BOLD/mmHg) and CVR delay, in breath-hold BOLD fMRI data, when $P_{ET}CO_2$ quality is low. In many cases, the participant performs all or most of the breath-hold trials in a session, but the $P_{ET}CO_2$ timeseries only shows an end-tidal CO_2 increase for a subset of the trials. This often occurs when a participant does not successfully exhale after the breath-hold period or breathes through their mouth in certain trials. In these cases, we expect the RVT timeseries to show large decreases corresponding to all or most of the breath-holds and the BOLD data to show signal increases, particularly in gray matter, during those same breath-holds. Here, we propose to make RVT have units of mmHg by rescaling it have the same minimum and maximum as a reliable portion of high-quality measured $P_{ET}CO_2$ (i.e., one successfully completed breath-hold trial). Rescaling RVT to mmHg will allow CVR to be calculated in units of %BOLD/mmHg.

Next, we will investigate whether using a $P_{ET}CO_2$ regressor predicted from RVT using deep learning produces more accurate maps of CVR amplitude and delay than the rescaled RVT regressor. As mentioned, Agrawal et al. (2023) previously used deep learning to predict $P_{ET}CO_2$ from RVT in resting-state data but found that their model performed poorly; we hypothesize that since breath holds evoke larger fluctuations in $P_{ET}CO_2$ than resting-state, breath-hold data will allow for more robust predictions of $P_{ET}CO_2$ than in their original work. Since the magnitude of arterial CO_2 varies significantly both within and between healthy participants and depends on a variety of factors such as the time of day, metabolism, sleep, and diet (Crosby & Robbins, 2004), and RVT is recorded in arbitrary units and varies with

changes in belt position and tightness, we will not use RVT to infer the magnitude of arterial CO_2. Instead, we will rescale the predicted $P_{ET}CO_2$ regressor to mmHg using the same methods used to rescale RVT. We hypothesize that the rescaled, predicted $P_{ET}CO_2$ regressor will allow for more accurate maps of CVR amplitude (%BOLD/mmHg) and delay than the rescaled RVT regressor.

Ultimately, we will evaluate the use of rescaled RVT and rescaled, predicted $P_{ET}CO_2$ regressors for mapping CVR in a subset of the publicly available EuskalIBUR dataset (Moia et al., 2020b), which provides breath-hold fMRI data for a group of densely-sampled participants. This dataset will allow us to comprehensively evaluate these strategies, ultimately providing guidance on the most robust method for mapping CVR in diverse clinical populations.

2. Methods

2.1. Data

2.1.1. In-house training dataset

To train a model to predict $P_{ET}CO_2$ and determine model hyperparameters, we compiled a large dataset of physiological recordings during various breath-holding protocols. This dataset is available on OSF at https://doi.org/10.17605/OSF.IO/Y5CK4 (Clements et al., 2024) and consists of 245 total datasets collected from 56 individuals (26 ± 4 years, 35 M) at Northwestern University under studies approved by the Northwestern University Institutional Review Board; all participants provided written, informed consent. Each dataset consisted of expired CO_2 pressure (mmHg) and respiration effort (arbitrary units) simultaneously recorded during a breath-hold task, described below. CO_2 pressure and respiration effort were recorded using a nasal cannula connected to an ADInstruments gas analyzer and a BIOPAC respiratory belt, respectively. Signals from the gas analyzer and respiratory belt were fed through PowerLab and recorded with LabChart (ADInstruments). All signals were acquired at 100 Hz.

This training dataset was collected using 4 different breath-hold tasks. All tasks had multiple breath-hold trials, each of which consisted of a breath hold, an exhalation, and a recovery period (all of varied lengths across tasks), and a period of paced breathing (always 3 seconds in, 3 seconds out). Some tasks also incorporated a period of rest before or after. The timings of each task and the number of datasets collected using each task are summarized in Table 1. Tasks 1 and 2 were acquired in the MRI scan environment and compiled from previous studies in our lab. Tasks 3 and 4 were acquired outside the

MRI environment specifically for this project. To ensure consistency across data collection environments, all participants were in the supine position and viewed the task stimuli on a monitor using a mirror. Stimuli were presented using PsychoPy (Peirce, 2007). Tasks 3 and 4 were designed to improve the generalizability of our modeling to any breath-hold task by incorporating randomized task timings. For each breath hold in Task 4, there was a 10% chance that the hold was skipped and replaced with a rest period, mimicking participants who fail to perform the trial (e.g., when falling asleep in the scanner).

Table 1. Task timings and number of datasets collected using each task

Task Number	1	2	3	4
Number of datasets	112	58	20	55
Initial rest period duration (s)	20	15	0	0
Number of trials	7	5	6	10
Paced breathing duration (s)	24	24	24	[24, 30, 36] randomized with replacement
Breath hold duration (s)	18	18	[10, 12, 14, 16, 18, 20] randomized without replacement, 10% chance that each breath hold is skipped and replaced with a rest period	[10, 11, 12, 13, 14, 15, 16, 17, 18, 19, 20] randomized with replacement
Exhalation duration (s)	2	3	2	2
Recovery duration (s)	6	6	6	[6, 7, 8, 9, 10, 11, 12] randomized with replacement
End rest period duration (s)	30	15	0	0

2.1.2. EuskalIBUR testing dataset

To evaluate our $P_{ET}CO_2$ prediction accuracy, as well as evaluate the performance of both rescaled RVT regressors and rescaled, predicted $P_{ET}CO_2$ regressors for mapping CVR in breath-hold fMRI data, we used the publicly available EuskalIBUR dataset that was acquired by researchers at a different institution. This breath-hold dataset consists of both physiological and MRI data. 10 participants (32 ± 6 years, 5M) completed 10 weekly MRI scan sessions each; every session included a breath-hold task during an fMRI scan. Data for 7 of the 10 participants can be found on OpenNeuro at doi:10.18112/openneuro.ds003192.v1.0.1 (Moia et al., 2020b). The total dataset size was 99 sessions due to a software malfunction during physiological data collection for subject 10, session 1. For details about the breath-hold task and multi-echo fMRI data acquisition, as well as the acquisition of single-band reference (SBRef) images, a T1-weighted MP2RAGE, and a T2-weighted Turbo Spin Echo image, readers are referred to Moia et al. (2021). During each fMRI scan, exhaled CO_2 was measured using a nasal cannula connected to an ADInstruments gas analyzer and transferred to a BIOPAC MP150 physiological monitoring system. Respiration effort was also measured; for the first 6-7 sessions (varied between subjects), a BIOPAC respiratory effort transducer connected to a BIOPAC respiration amplifier was used, and for the remaining sessions a BIOPAC pressure pad and transducer amplifier were used. All signals were acquired at 10 kHz and down sampled to 100 Hz before any additional processing was performed.

2.1.3. Physiological data processing and evaluation

All CO_2 and respiratory belt data in both the training and testing dataset were processed using in-house MATLAB code (MathWorks, Natick, MA, R2022b). For the CO_2 data, a peak-detection algorithm identified end-tidal peaks. The results of the algorithm were manually verified, and the peaks were linearly interpolated to create $P_{ET}CO_2$ timeseries with the same frequency as the original CO_2 data. $P_{ET}CO_2$ timeseries were rescaled from units of Volts to mmHg using instructions from the manufacturer of the gas analyzer. For the respiratory belt data, alternating minima and maxima were identified using a peak-detection algorithm, manually verified, and used to calculate respiration volume per time (RVT) based on the method described by Birn et al. (2006). The RVT estimations were linearly interpolated to create RVT timeseries with the same frequency as the original respiratory belt data. Since this method requires alternating minima and maxima, we accounted for having two consecutive minima due to exhales before and after the breath hold by only included minima before the hold (Zvolanek et al., 2023).

Next, we assessed $P_{ET}CO_2$ data quality to ensure that only high-quality breath holds were used to train the model and evaluate model predictions. To assess $P_{ET}CO_2$ quality, the $P_{ET}CO_2$ change induced by each breath hold was calculated; a large $P_{ET}CO_2$ change indicates a high-quality measurement since breath-holding causes CO_2 to accumulate in the blood (Tancredi & Hoge, 2013). A custom script was developed that identified the peaks in the raw CO_2 timeseries that were immediately before and after each breath hold. Then, the change in CO_2 induced by each breath hold was calculated as the difference in amplitude between the peaks in each pair. Among breath-holds causing positive CO_2 changes, the mean and standard deviation CO_2 increase was calculated. Breath holds that caused a CO_2 increase greater than the mean minus 1 standard deviation were classified as "high-quality." This threshold was chosen with the aim of classifying the majority of breath-holds that caused any CO_2 increase as high-quality, while still excluding breath-holds that caused CO_2 increases substantially lower than average. These low CO_2 increases were likely due to participants breathing through their mouth or not fully exhaling after the breath-hold. After quality assessment, $P_{ET}CO_2$ and RVT timeseries were downsampled to 10 Hz.

Next, we needed to account for delays between $P_{ET}CO_2$ and RVT, related to measurement delays caused by factors such as sample line lengths, as well as physiological delays between changes in respiratory volume and subsequent changes in arterial CO_2. Therefore, each $P_{ET}CO_2$ dataset was shifted to maximize its negative cross-correlation with each RVT dataset. A negative correlation between $P_{ET}CO_2$ and RVT is expected because breath holds cause simultaneous increases in arterial CO_2 and decreases in respiratory volume. Because we expected the measurement delay to be greater for $P_{ET}CO_2$ than RVT, we only allowed for negative shifts, meaning that $P_{ET}CO_2$ could only be shifted earlier in time. For all $P_{ET}CO_2$ recordings, the maximum allowable shift was 30 seconds. This maximum shift was identified through trial and error to ensure that all of the calculated shifts were not consistently at the maximum value. After each $P_{ET}CO_2$ timeseries was shifted, data were trimmed from the end of the corresponding RVT signal to ensure that it was the same length as the shifted $P_{ET}CO_2$ timeseries.

Lastly, all $P_{ET}CO_2$ and RVT recordings were z-normalized (i.e., zero mean and unit standard deviation). The RVT timeseries were z-normalized to avoid biasing the model, since RVT is derived from respiration effort data that are recorded in arbitrary units. $P_{ET}CO_2$ timeseries were also z-normalized because, as previously explained, the

magnitude of arterial CO_2 cannot be inferred from RVT alone, and the scaling between these data types will likely vary between individuals.

We chose not to convolve RVT or $P_{ET}CO_2$ with response functions, despite the fact that this is required for CVR calculation. $P_{ET}CO_2$ is often convolved with the canonical hemodynamic response function (HRF) consisting of the sum of two gamma functions (Friston et al., 1998); however, this may not be a universally optimal approach as the shape of the HRF is known to vary across subjects and brain regions (Handwerker et al., 2004). Additionally, the canonical HRF was designed to model the BOLD response to neural activity, not a CO_2 change, and these responses have been shown to exhibit different shapes (Golestani et al., 2015). Similarly, RVT is often convolved with the respiration response function (RRF) (Birn et al., 2008), which was designed to model the average respiration-induced response function across the brain and does not account for variations in the shape of the response across subjects or brain regions. Developing a model that could predict $P_{ET}CO_2$ before convolution provides the flexibility to choose any response function before calculating CVR.

2.1.4. MRI pre-processing

MRI data were pre-processed for each scan session in which the associated $P_{ET}CO_2$ trace had all high-quality breath holds and for 2 additional scan sessions in which the majority of breath holds were low-quality. Pre-processing was performed using custom scripts which follow the same key steps described in Zvolanek et al. (2023). Scripts are available at https://github.com/BrightLab-ANVIL/PreProc_BRAIN and utilize both FSL (Cox, 1996; Jenkinson et al., 2012) and AFNI (Cox, 1996) commands. In summary, motion realignment, brain extraction, optimal combination of the echoes using tedana (DuPre et al., 2021; Kundu et al., 2012, 2013), and distortion correction were performed on the fMRI data. The MP2RAGE was brain extracted and used to generate a gray matter mask which was transformed into functional space.

2.2. Experiments

2.2.1. Prediction of $P_{ET}CO_2$ from RVT

To model $P_{ET}CO_2$ from RVT, we used a 1D fully convolutional network (FCN), which is a type of convolutional neural network that does not have any fully connected layers.

2.2.1.1. Implementation details

We segmented our delay-corrected, z-normalized training datasets into smaller data segments containing only high-quality breath holds so that we could make use of CO_2 recordings containing poorly performed breath-hold trials and maximize the size of our overall training dataset. Additionally, this method ensured that our model was generalizable to breath-hold tasks of varying lengths. High quality breath-holds were identified using the methods outlined in Section 2.1.3; the skipped breath holds from Task 4 were also classified as high-quality so that they could be included in the training dataset.

Next, $P_{ET}CO_2$ data were separated into blocks, each containing one breath hold. To ensure we captured the CO_2 build-up and recovery effectively, we included data from before and after the apneic period. To identify the data that could be included in each segment, we calculated the halfway point between the end of each breath hold and the start of the next breath hold. Each block contained data from one halfway point to the next. We also manually estimated the start and end period of each skipped breath hold from Task 4 to create skipped breath-hold blocks that were still included in the training dataset. For blocks containing the first or the last trial in a dataset, we included all remaining data at the start or end of the trace, respectively. Using these breath-hold blocks, each $P_{ET}CO_2$ dataset was randomly segmented into 1–4 different data segments of varying lengths; each segment contained 2 or more consecutive, high-quality breath-hold blocks.

2.2.1.2. Model optimization

The input to the FCN is an N x 2 array and the output predicted $P_{ET}CO_2$ is an N x 1 array. The first column of the input is the z-normalized, N-long RVT trace, and the second column is the subject ID encoded using one-hot encoding (Paszke et al., 2019) and padded with zeroes to be N samples long. Subject ID was inputted to the model to account for the fact that most participants contributed multiple datasets and to encourage the model to learn subject-specific differences between physiological timeseries. Upon being inputted to the model, the z-normalized RVT trace was further normalized using the *tanh* operator to ensure that all values were between -1 and 1 (Agrawal et al., 2023).

Several FCNs with varying numbers of hidden layers were initially investigated. Using methods described by Agrawal et al., who examined a similar relationship between physiological recordings in free (resting-state) breathing, we created FCNs

with 1, 2, 4, and 6 convolutional layers; this code is available at https://github.com/vismayagrawal/RESPCO. However, because overfitting was not initially observed with the 6 convolutional layer model, we also created FCNs with 8, 10, 12, and 14 layers. For all models, half the layers were convolutional, and the other half were transposed convolutional. Both convolution and transposed convolution were performed using a stride of 2.

Each FCN used an adaptive learning rate that was implemented using Pytorch's ReduceLROnPlateau command; the initial learning rate was 0.01, and this learning rate was reduced by a factor of 0.1 if improvements were not seen for 4 consecutive epochs (Paszke et al., 2019). Additionally, each FCN had a batch size of 1 and used the Adam optimization algorithm during training (Kingma & Lei Ba, 2015).

In addition to investigating different numbers of layers, we also investigated using 5, 10, 15, 20, and 25 epochs. For the loss function, we used mean squared error (MSE) between the measured and predicted $P_{ET}CO_2$ timeseries but, similarly to Agrawal et al. (2023), observed that when using MSE as the loss function, the FCN consistently underestimated the peaks in the data. In $P_{ET}CO_2$ timeseries, the values at the peaks are important since they indicate the extent of hypercapnia induced by each breath hold. Therefore, in addition to testing standard MSE, we tested four additional loss functions. These loss functions simply add the MSE at the peaks in the measured $P_{ET}CO_2$ trace, multiplied by a factor of either 0.5, 1, 1.5, or 2, to the standard MSE calculated using the entire $P_{ET}CO_2$ trace. Peaks were automatically identified using the *Peakutils* Python package. 5-fold cross validation was used to ensure a robust estimation of model performance for each possible hyperparameter combination, with 80% and 20% of the data segments assigned to the training and test sets, respectively, at each fold.

For each possible model, we compared the ground truth and predicted $P_{ET}CO_2$ traces by calculating the average and standard deviation of the Pearson correlations transformed to Fisher's Z across the 5 folds. We also calculated the average and standard deviation mean absolute error (MAE), MSE, and MSE at each of the peaks across the five folds. As described above, the height of the $P_{ET}CO_2$ peaks provides valuable information about the extent of hypercapnia during the breath hold, which is critical for accurately modeling CVR. Therefore, the hyperparameter combination that resulted in the lowest average MSE at the peaks was considered optimal.

2.2.1.3. Generation of predicted $P_{ET}CO_2$ timeseries

Using the optimal hyperparameters, we trained the FCN using the entire training dataset. After training was completed, the RVT timeseries and subject IDs for each subject in the testing dataset were inputted to the model to produce predicted $P_{ET}CO_2$ timeseries for each subject and session. A summary of the methods for implementing and optimizing the FCN and generating predicted $P_{ET}CO_2$ timeseries is provided in Figure 1.

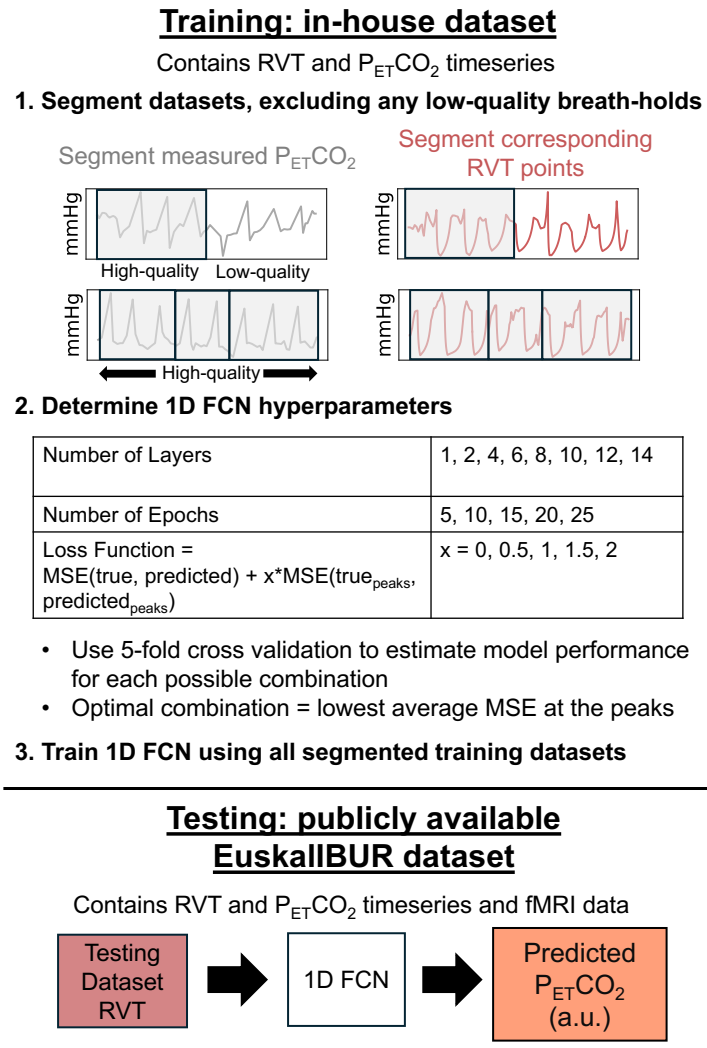

Figure 1. Overview of the methods for training and evaluating a 1D FCN to predict $P_{ET}CO_2$ from RVT. Training datasets were randomly separated into 1-4 smaller data segments, excluding any low-quality breath holds. Optimal hyperparameters were identified by using 5-fold cross-validation to estimate model performance for each possible combination, and the model was trained using the optimal hyperparameter

combination. Next, the RVT timeseries in the test dataset, along with subject ID (not shown in the figure), were inputted to the model to generate $P_{ET}CO_2$ predictions in arbitrary units (a.u.).

2.2.2. Rescaling of RVT and predicted $P_{ET}CO_2$ timeseries in the test set

Here, we investigated whether measured $P_{ET}CO_2$ data for one or more high-quality breath holds could be used to rescale RVT and predicted $P_{ET}CO_2$ to units of mmHg. Individual breath-hold blocks (see Section 2.2.1.1), which included measured $P_{ET}CO_2$ data before, during, and after each high-quality breath hold, were used for rescaling. Both predicted $P_{ET}CO_2$ and RVT were rescaled to have the same minimum and maximum as the first (high-quality) breath-hold block in the measured $P_{ET}CO_2$ timeseries. To better understand whether using more breath-hold blocks increased the rescaling accuracy, we also rescaled $P_{ET}CO_2$ and RVT to have the same minimum and maximum as the first 2 sequential high-quality breath-hold blocks and the first 3 sequential high-quality breath-hold blocks. The result was three different sets of rescaled, predicted $P_{ET}CO_2$ and rescaled RVT regressors that were rescaled using high-quality measured $P_{ET}CO_2$ data from 1, 2, or 3 sequential breath-hold trials.

2.2.3. Evaluation of rescaled RVT and rescaled, predicted $P_{ET}CO_2$ timeseries

Next, we assessed the error of rescaled RVT and rescaled, predicted $P_{ET}CO_2$ relative to measured $P_{ET}CO_2$. In these calculations, we only included datasets in which all of the breath holds in the measured $P_{ET}CO_2$ timeseries were classified as high-quality, meaning that these measured $P_{ET}CO_2$ timeseries could be used as ground truths. One caveat is that RVT is expected to be negatively correlated with measured $P_{ET}CO_2$, while predicted $P_{ET}CO_2$ is expected to be positively correlated with measured $P_{ET}CO_2$. To allow for fair comparisons and consistency with how these timeseries are typically processed in fMRI research, each measured and rescaled, predicted $P_{ET}CO_2$ timeseries was convolved with the canonical HRF (Friston et al., 1998) and each rescaled RVT timeseries was convolved with the RRF (Birn et al., 2008). This made all of the timeseries positively correlated with each other, but the RRF and HRF have different latencies. Therefore, to evaluate rescaled RVT relative to measured $P_{ET}CO_2$, rescaled RVT timeseries convolved with the RRF were also shifted later in time (maximum shift = 30 seconds) to maximize their positive correlation with measured $P_{ET}CO_2$. To ensure that all signals being compared were the same length, measured and rescaled, predicted $P_{ET}CO_2$ timeseries, both convolved with

the HRF, were trimmed to match the length of the shifted RVT timeseries convolved with the RRF.

To compare the strength of the relationships between RVT and measured $P_{ET}CO_2$, as well as between predicted $P_{ET}CO_2$ and measured $P_{ET}CO_2$, we calculated the mean and standard deviation Pearson's correlation transformed to Fisher's Z. Additionally, to evaluate the magnitude of differences between these metrics, we computed the average and standard deviation of the mean absolute error (MAE), mean squared error (MSE), and MSE at the peaks of RVT and predicted $P_{ET}CO_2$ relative to measured $P_{ET}CO_2$ for each rescaling method.

Next, we conducted a 2-sided paired *t*-test (significance threshold $p<0.05$) to assess whether the correlations of RVT and predicted $P_{ET}CO_2$ to measured $P_{ET}CO_2$ were significantly different; only 1 *t*-test was needed since correlation is not affected by rescaling. For each error term (MAE, MSE, and MSE at the peaks), a 2-sided paired *t*-test was conducted to compare the errors for RVT and predicted $P_{ET}CO_2$ for each rescaling method, resulting in 3 tests for each error term. To understand if using more than 1 breath hold for rescaling was beneficial, 4 additional 2-sided paired *t*-tests were conducted for each error term to compare the errors of RVT rescaled using 1 and 2 breath holds, RVT rescaled using 2 and 3 breath holds, predicted $P_{ET}CO_2$ rescaled using 1 and 2 breath holds, and predicted $P_{ET}CO_2$ rescaled using 2 and 3 breath holds. For these tests, we used a significance threshold of $p<0.05$, with Bonferroni correction to account for doing 7 total tests for each error term.

Lastly, to better understand our model's $P_{ET}CO_2$ prediction performance, we also calculated the normalized correlation, MAE, MSE, and MSE at the peaks of measured and predicted $P_{ET}CO_2$ before either signal was convolved with the HRF, since convolution with the HRF can improve relationships between signals.

2.2.4. Estimation of CVR amplitude and delay

For each pre-processed scan session, 7 different regressors were used for 7 separate CVR calculations. These regressors were measured $P_{ET}CO_2$, predicted $P_{ET}CO_2$ rescaled using 1 breath hold, predicted $P_{ET}CO_2$ rescaled using 2 breath holds, predicted $P_{ET}CO_2$ rescaled using 3 breath holds, RVT rescaled using 1 breath hold, RVT rescaled using 2 breath holds, and RVT rescaled using 3 breath holds. Measured and predicted $P_{ET}CO_2$ regressors were convolved with the canonical HRF (Friston et al., 1998) and RVT regressors were convolved with the RRF (Birn et al., 2008). A summary of the methods

used to generate these CVR regressors is shown in Figure 2. Voxelwise maps of CVR amplitude and delay were generated for each regressor with phys2cvr (Moia et al., 2024) using a temporal lag range of ±9 seconds in 0.3 second shift increments. For details about the lagged general linear model approach used by phys2cvr, readers are referred to Moia et al. (2020). In addition to modeling shifted variants of the $P_{ET}CO_2$ trace in our GLMs, we also modeled Legendre polynomials up to 4th order and 6 demeaned motion parameters with each of their associated temporal derivatives. The delay maps were normalized by being recentered on the median delay in gray matter, and then the amplitude and normalized delay maps were thresholded to remove voxels with delay values at the boundary conditions (-9, -8.7, 8.7, or 9 s) since they were considered not optimized (Moia et al., 2020a). Lastly, amplitude and delay maps were registered to MNI space using the FSL 1mm MNI template resampled to 2.5mm resolution (FLIRT and FNIRT, FSL).

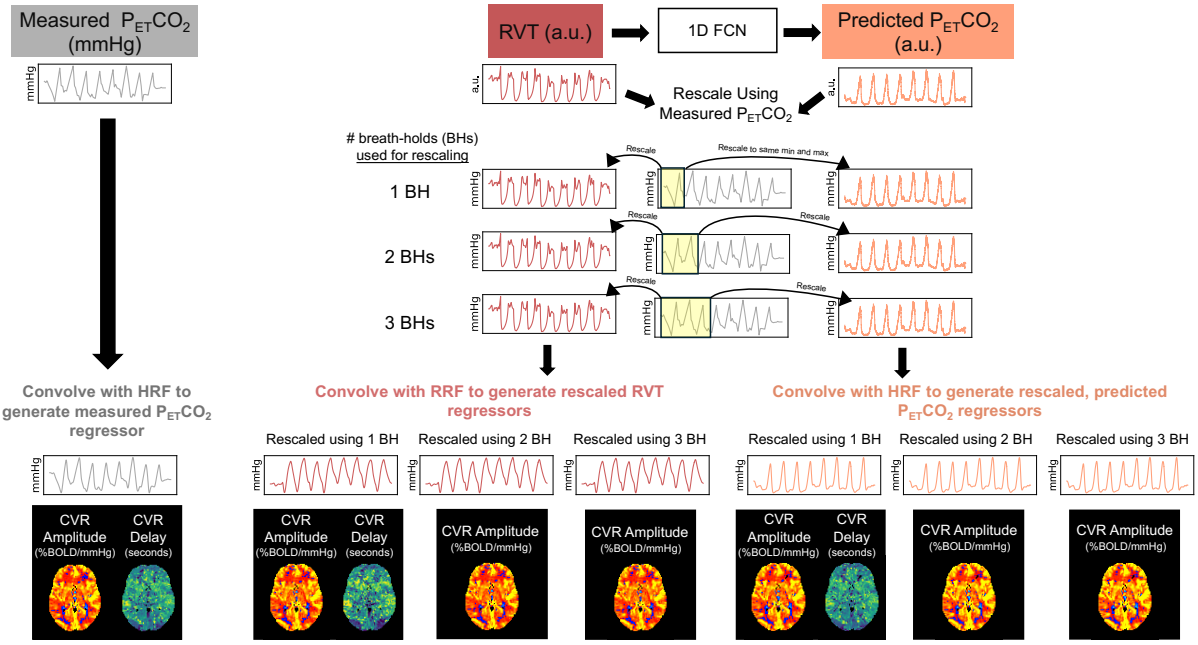

Figure 2. Overview of the methods pipeline for generating regressors to map CVR. Measured $P_{ET}CO_2$ was convolved with the canonical hemodynamic response function (HRF) and used to map CVR amplitude and delay. In datasets with $P_{ET}CO_2$ timeseries containing only high-quality breath-holds, these maps served as ground truths. RVT was used as an input to a 1D FCN to generate predicted $P_{ET}CO_2$ timeseries in arbitrary units (a.u.). Both RVT and predicted $P_{ET}CO_2$ were rescaled to mmHg using 1, 2, and 3 breath-holds in the measured $P_{ET}CO_2$ timeseries. Rescaled RVT and rescaled, predicted $P_{ET}CO_2$ were convolved with the respiration and hemodynamic response functions, respectively, and used to map CVR. Note that CVR delay is not sensitive to rescaling, so only 1 delay map each was generated for RVT and predicted $P_{ET}CO_2$.

2.2.5. Analysis of CVR amplitude and delay maps for datasets with all high-quality breath holds

Datasets with measured $P_{ET}CO_2$ timeseries containing only high-quality breath holds provided CVR amplitude and delay maps that served as ground truths. Among these datasets, we calculated 6 group-level MAE maps to show CVR amplitude errors due to the choice of regressor (predicted $P_{ET}CO_2$ or RVT) and the choice of rescaling method (1, 2, or 3 breath holds) relative to the ground truth maps. As CVR delay maps are not sensitive to the rescaling method, we also generated 2 MAE maps to show differences between delay maps generated using predicted $P_{ET}CO_2$ or RVT and ground truth delay maps. For each MAE map, the median MAE in gray matter was calculated.

To better understand errors in scan-level CVR amplitude estimations related to the choice of regressor and the rescaling method, we also calculated the median absolute error in gray matter for each individual CVR amplitude map relative to the ground-truth map. The distribution of errors was plotted for each regressor and rescaling method, and significant differences between distributions were evaluated using Wilcoxon signed-rank tests. 7 total tests were conducted to compare the amplitude values for predicted $P_{ET}CO_2$ and RVT for each rescaling method and assess changes in error associated with rescaling using 2 breath holds instead of 1 and 3 breath holds instead of 2 for both predicted $P_{ET}CO_2$ and RVT (significance level $p<0.05$, Bonferroni corrected).

Lastly, we assessed how well the predicted $P_{ET}CO_2$ and RVT regressors maintain the ranking of CVR amplitude values across subjects and scan sessions. Specifically, we wanted to confirm that if a subject exhibited a particularly high or low CVR value for a particular scan compared to other scans, this subject would also show a relatively high or low CVR value in maps generated using the rescaled, predicted $P_{ET}CO_2$ and rescaled RVT regressors. To assess this, the Spearman Rank Correlation was calculated to compare the rankings of median CVR amplitudes in gray matter for measured $P_{ET}CO_2$ (ground truth) and RVT amplitude maps, as well as measured $P_{ET}CO_2$ and predicted $P_{ET}CO_2$ amplitude maps. This analysis was performed for RVT and predicted $P_{ET}CO_2$ regressors rescaled using 1, 2, and 3 breath holds.

2.2.6. Analysis of CVR amplitude and delay maps in datasets with mostly low-quality breath holds

We also evaluated the effectiveness of using a rescaled RVT and rescaled, predicted $P_{ET}CO_2$ regressor in 2 example datasets in which the RVT timeseries indicated that the participant attempted every breath hold in the task, but the $P_{ET}CO_2$ timeseries contained mostly low-quality breath holds (likely due to the participant not exhaling immediately after each breath hold). For each CVR amplitude and delay map generated using RVT and predicted $P_{ET}CO_2$, we calculated the spatial correlation in gray matter (3ddot, AFNI) relative to the ground truth maps. For each scan, the ground truth maps were from a different session for the same subject that had a measured $P_{ET}CO_2$ trace containing only high-quality breath holds.

2.2.7. Case study in a participant with Moyamoya disease

To evaluate the clinical utility of using rescaled RVT and rescaled, predicted $P_{ET}CO_2$ regressors to map CVR, we also scanned a 31-year-old male with unilateral Moyamoya disease causing an occluded right middle cerebral artery. This participant completed a breath-hold task during a functional T2*-weighted scan which used a multi-echo, gradient-echo EPI sequence (CMRR, Minnesota) on a 3T Siemens Prisma. The functional scan parameters and breath-hold task were similar to those in the EuskalIBUR dataset (Moia et al., 2020b, 2021). A whole brain T1-weighted EPI-navigated multi-echo MPRAGE scan, based on Tisdall et al. (2016), was also acquired with scan parameters previously described by Stickland et al. (2021).

Exhaled CO_2 and respiration effort timeseries were recorded and processed (see Sections 2.1.1 and 2.1.3, respectively, for methods), and predicted $P_{ET}CO_2$ timeseries were generated (Section 2.2.1.3). Predicted $P_{ET}CO_2$ and RVT were rescaled using measured $P_{ET}CO_2$ data for 1 high-quality breath hold (Section 2.2.2). fMRI data were pre-processed using similar methods as those described in Section 2.1.4. CVR amplitude and delay maps were calculated for the measured $P_{ET}CO_2$, rescaled, predicted $P_{ET}CO_2$, and rescaled RVT regressors using the methods described in Section 2.2.4, with two exceptions to account for the expected increase in CVR delays due to Moyamoya pathology: a maximum lag value of ±15 seconds was used, and maps were not thresholded to remove voxels with delay values at the boundaries (-15, -14.7, 14.7, 15).

For both CVR amplitude and delay, within a gray matter mask, we evaluated the spatial correlation of the maps generated using rescaled, predicted $P_{ET}CO_2$ and rescaled RVT relative to the ground truth amplitude and delay maps generated using measured $P_{ET}CO_2$. Because we expected longer CVR delays in the right MCA territory in this

participant (Stickland et al., 2021), we also specifically assessed whether the RVT and predicted $P_{ET}CO_2$ methods could be used to effectively identify brain areas with extreme delays. To identify these areas, we thresholded the delay maps to only contain voxels with delay values greater than or equal to 10 seconds, and then made a binarized map of clusters with at least 15 voxels (3dClusterize, AFNI). Then, we calculated the Dice similarity coefficient between the clusters in the rescaled RVT delay map or the rescaled, predicted $P_{ET}CO_2$ delay map and the clusters in the measured $P_{ET}CO_2$ map (the ground truth).

3. Results

3.1. Physiological data processing and evaluation

In the in-house training dataset, the average CO_2 change across all breath holds was 9.85 ± 4 mmHg. Any breath hold that resulted in a CO_2 increase greater than 6.33 mmHg (the mean CO_2 increase minus 1 standard deviation) was considered high-quality. In the EuskalIBUR test dataset, the average CO_2 increase induced by a breath hold was 6.73 ± 3 mmHg and high-quality breath-hold trials needed to cause a CO_2 increase greater than 3.60 mmHg.

We observed similar task compliance trends in the training and test datasets. In the training dataset, 53% of the 245 total CO_2 recordings contained all high-quality breath holds, and 4.5% of the CO_2 recordings contained no high-quality breath holds (Figure 3A). In the test dataset, 57% of the 99 total recordings contained entirely high-quality breath-hold trials, while 7% contained no high-quality breath-hold trials (Figure 3B).

Each $P_{ET}CO_2$ timeseries was shifted to account for delays between $P_{ET}CO_2$ and RVT. In the training and test datasets, $P_{ET}CO_2$ was shifted an average of 16.0 ± 4 and 23.4 ± 5 seconds earlier, respectively, to maximize its negative cross-correlation with RVT. Using the temporal location of each high-quality breath hold in each $P_{ET}CO_2$ timeseries in the training dataset (after accounting for the applied temporal shift), delay-corrected $P_{ET}CO_2$ and RVT timeseries in the training dataset were randomly segmented into 1-4 data segments consisting of consecutive, high-quality breath holds. After segmentation, the final size of the training dataset was 340 sets of $P_{ET}CO_2$ and RVT segments.

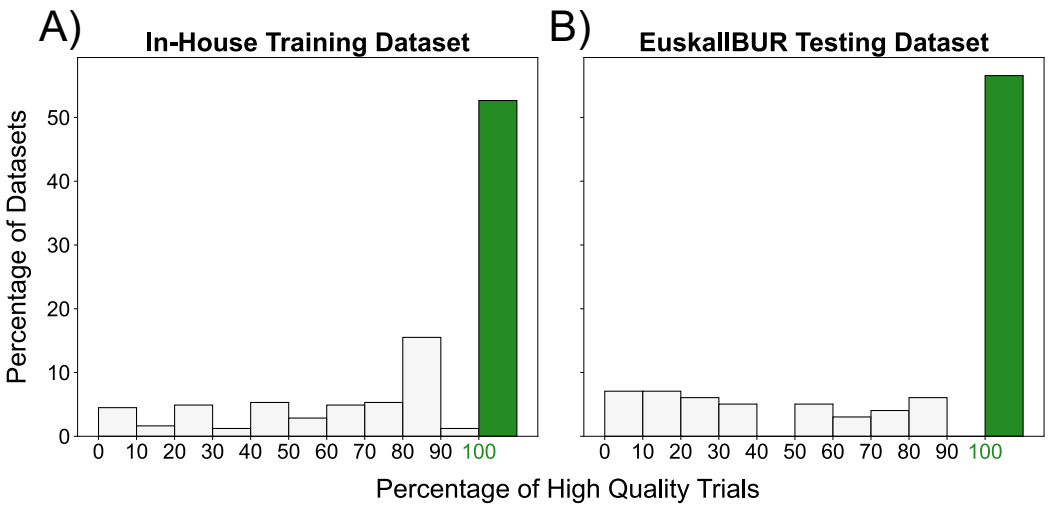

Figure 3. Distributions of the percentage of high-quality breath-hold trials out of the total number of trials in the in-house training dataset (A) and the EuskalIBUR testing dataset (B). For the training and EuskalIBUR datasets, high-quality breath holds are defined as trials resulting in CO_2 increases greater than 6.33 and 3.60 mmHg, respectively. Each bar includes the lower value and excludes the upper value of the interval. For example, the first bar of each histogram represents [0,10). The green bar indicates the percentage of CO_2 recordings containing only high-quality trials.

3.2. Model optimization

The model which resulted in the lowest MSE at the peaks, and consequently was considered the optimal model, used 12 layers, 20 epochs, and a loss function which summed the standard MSE (calculated using all datapoints) with the MSE at the peaks scaled by 0.5. Averaged across all 5 folds, this model resulted in a mean Fisher's Z of 1.34 ± 0.241, an MAE of 0.431 ± 0.114 (a.u.), an MSE of 0.352 ± 0.160 (a.u.), and an MSE at the peaks of 0.508 ± 0.999 (a.u.).

3.3. Evaluation of rescaled RVT and rescaled, predicted $P_{ET}CO_2$ timeseries

The EuskalIBUR testing dataset (unused during optimization and training of the $P_{ET}CO_2$ prediction model) was used to evaluate the rescaled RVT and rescaled, predicted $P_{ET}CO_2$ timeseries relative to measured $P_{ET}CO_2$. Figure 4 shows example measured $P_{ET}CO_2$ timeseries plotted against predicted $P_{ET}CO_2$ and RVT timeseries, both of which were rescaled using 1 breath hold. Examples are provided for both measured $P_{ET}CO_2$ timeseries with only

high-quality breath holds (Figure 4A) and measured $P_{ET}CO_2$ timeseries with mostly low-quality breath holds (Figure 4B).

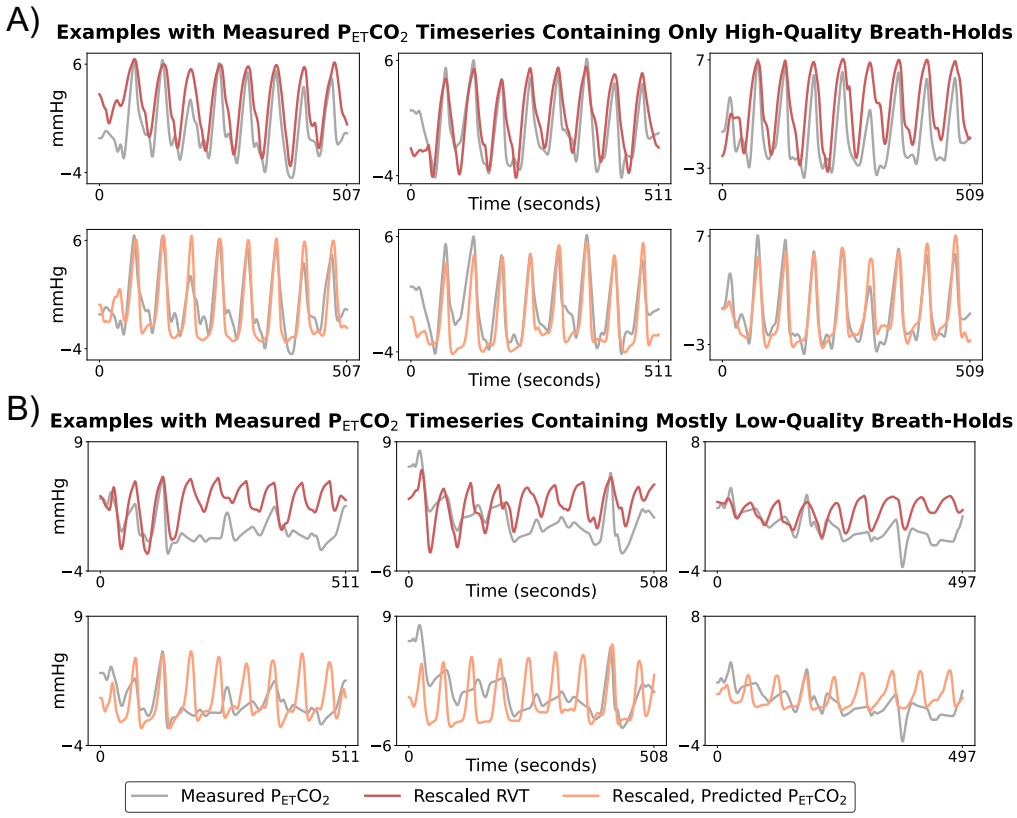

Figure 4. Example rescaled, predicted $P_{ET}CO_2$ and rescaled RVT timeseries (rescaled using 1 breath hold) plotted against measured $P_{ET}CO_2$ timeseries. Results are shown for 3 datasets in which the measured $P_{ET}CO_2$ had all high-quality breath holds (A) and 3 datasets with multiple low-quality breath holds (B).

Only datasets with measured $P_{ET}CO_2$ timeseries containing all high-quality breath holds were considered to be reasonable ground truths and were included in the following analysis (N=56). We compared rescaled RVT and rescaled, predicted $P_{ET}CO_2$ timeseries to measured $P_{ET}CO_2$ using a Pearson correlation normalized to Fisher's Z, MAE, MSE, and MSE at the peaks (Figure 5). Predicted $P_{ET}CO_2$ had a significantly higher correlation with measured $P_{ET}CO_2$ than RVT (p<0.05). Across the 3 rescaling methods, RVT had a significantly higher MAE and MSE than predicted $P_{ET}CO_2$ (p<0.05, Bonferroni corrected); the MSE at the peaks for predicted $P_{ET}CO_2$ was not significantly different than for RVT for any of the rescaling methods. For rescaling predicted $P_{ET}CO_2$, using 2 breath holds compared to 1 breath hold

significantly decreased the MAE (p<0.05, Bonferroni corrected) but not the MSE or MSE at the peaks; using 3 breath holds compared to 2 did not significantly impact any measures of error. For RVT, rescaling using 2 breath holds compared to 1 breath hold and 3 breath holds compared to 2 breath holds did not significantly change any measures of error.

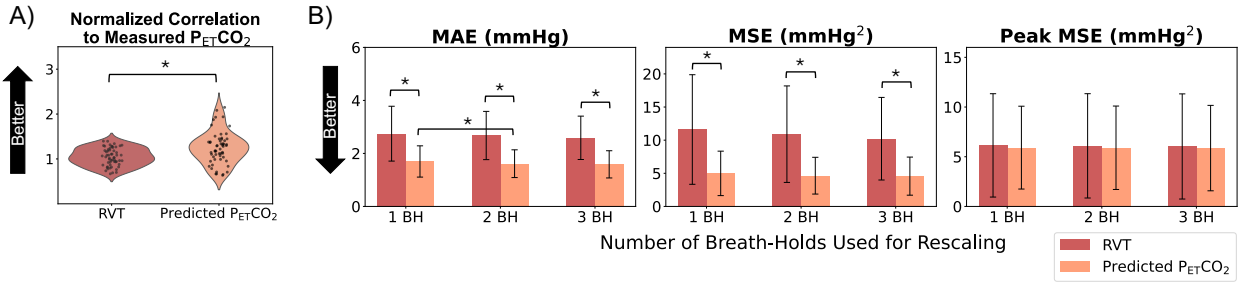

Figure 5. Overview of metrics comparing rescaled, predicted $P_{ET}CO_2$ and rescaled RVT to measured $P_{ET}CO_2$ in datasets in which all breath holds in the measured $P_{ET}CO_2$ timeseries were classified as high-quality. Both Fisher's Z values (A), which are not affected by rescaling, and error terms for each rescaling method (B) are shown. Asterisks indicate significant differences.

To gain a better understanding of our model's performance, we also assessed the correlation and error of predicted $P_{ET}CO_2$ relative to measured $P_{ET}CO_2$ before either signal was convolved with the HRF (Supplementary Figure S1). As expected, the mean normalized correlation of the unconvolved timeseries was slightly lower than that of the convolved timeseries (1.14 ± 0.3 compared to 1.24 ± 0.4); however, a normalized correlation of 1.14 still indicates strong $P_{ET}CO_2$ prediction performance. The error terms before and after convolution were relatively similar. These results demonstrate that our $P_{ET}CO_2$ prediction method is not restricted to the canonical HRF and that any appropriate response function can be effectively utilized with this approach.

3.4. CVR amplitude and delay maps for scans with all high-quality breath holds

For scan sessions with $P_{ET}CO_2$ timeseries containing all high-quality breath holds, CVR amplitude maps (in %BOLD/mmHg) generated using RVT and predicted $P_{ET}CO_2$ regressors, rescaled using 1 breath hold, appear similar (i.e., show similar amplitude patterns across the brain and have similar amplitude magnitudes) to the ground-truth maps generated using the measured $P_{ET}CO_2$ regressors (Figure 6). Similarly, the associated rescaled RVT and rescaled, predicted $P_{ET}CO_2$ CVR delay maps (in seconds, normalized to median gray matter delay)

appear similar to the ground-truth measured $P_{ET}CO_2$ CVR delay maps (Figure 7). The delay maps generated using rescaled, predicted $P_{ET}CO_2$ seem to better estimate extreme negative or positive delay values (voxels that are yellow or dark purple) in the ground truth delay map than the rescaled RVT maps. This is particularly evident in the delay maps for subject 10 session 4. Additionally, the delay maps generated using RVT appear to introduce extreme delay values that are not present in the ground truth maps, as seen in the left posterior portion of the delay map for subject 3 session 2.

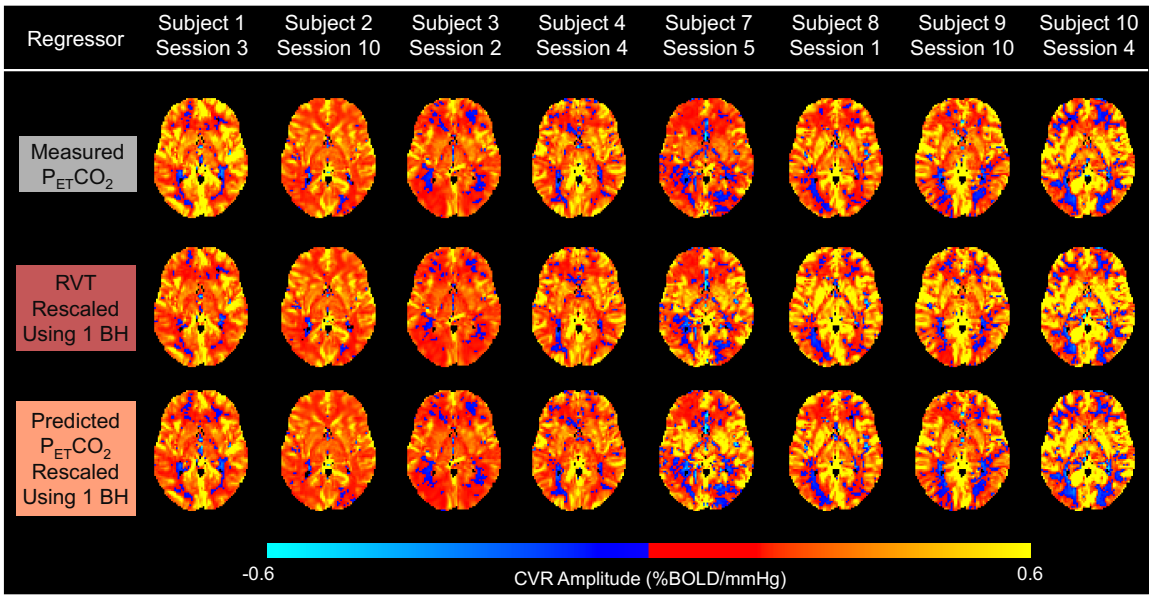

Figure 6. Example CVR amplitude maps for 8 subjects for sessions with measured $P_{ET}CO_2$ timeseries containing all high-quality breath holds (BHs). The top row shows ground truth amplitude maps, generated using the measured $P_{ET}CO_2$ regressor, while the middle and bottom rows show maps generated using rescaled RVT and rescaled, predicted $P_{ET}CO_2$ regressors, respectively.

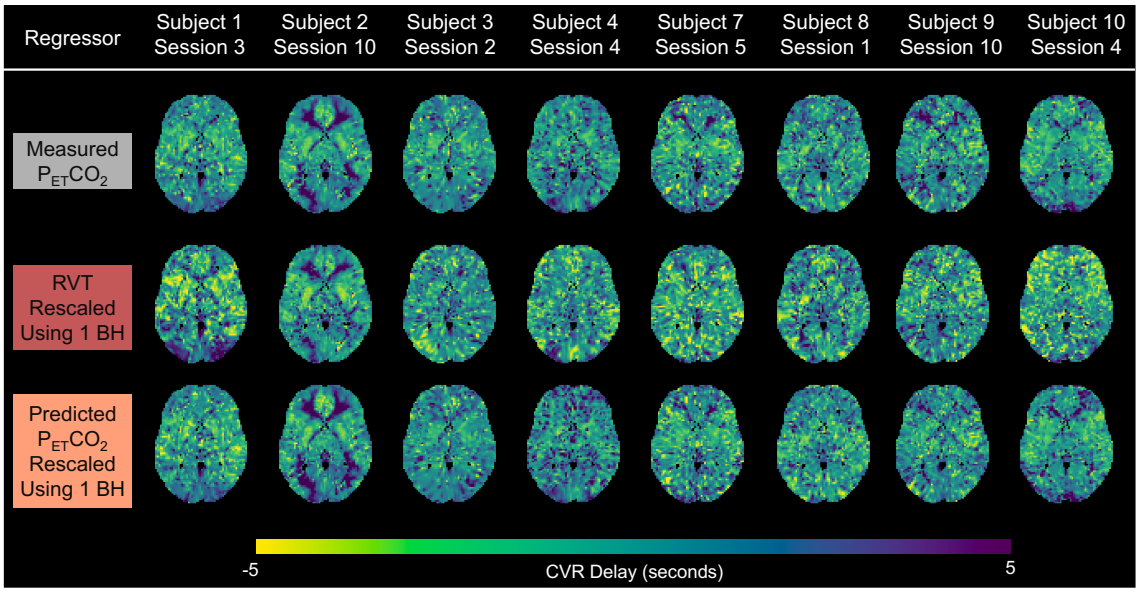

Figure 7. Example CVR delay maps for 8 subjects for sessions with measured $P_{ET}CO_2$ timeseries containing all high-quality breath holds (BHs). Ground truth delay maps, generated using the measured $P_{ET}CO_2$ regressor, are shown in the top row, while delay maps generated using rescaled RVT and rescaled, predicted $P_{ET}CO_2$ regressors are shown in the middle and bottom rows, respectively. Delay maps are normalized to the gray matter median. Negative delays reflect earlier responses, while positive delays reflect later responses.

Next, to better understand the impact of the rescaling method on CVR accuracy, group-level MAE maps were computed to assess the errors in CVR amplitude maps generated using RVT and predicted $P_{ET}CO_2$ regressors, rescaled using 1, 2, and 3 breath holds, relative to the ground truth maps generated using measured $P_{ET}CO_2$ (Figure 8). Across the 3 rescaling methods, the median MAE in gray matter is consistently lower for rescaled, predicted $P_{ET}CO_2$ than for RVT. In each map, the magnitude of the error appears consistent throughout gray matter, suggesting that the CVR amplitude bias introduced by the RVT and predicted $P_{ET}CO_2$ regressors is not specific to any part of the cortex. Increasing the number of breath holds used to rescale RVT slightly decreased the median MAE in gray matter. Rescaling predicted $P_{ET}CO_2$ using 2 breath holds compared to 1 but not 3 breath holds compared to 2 slightly decreased the median MAE in gray matter.

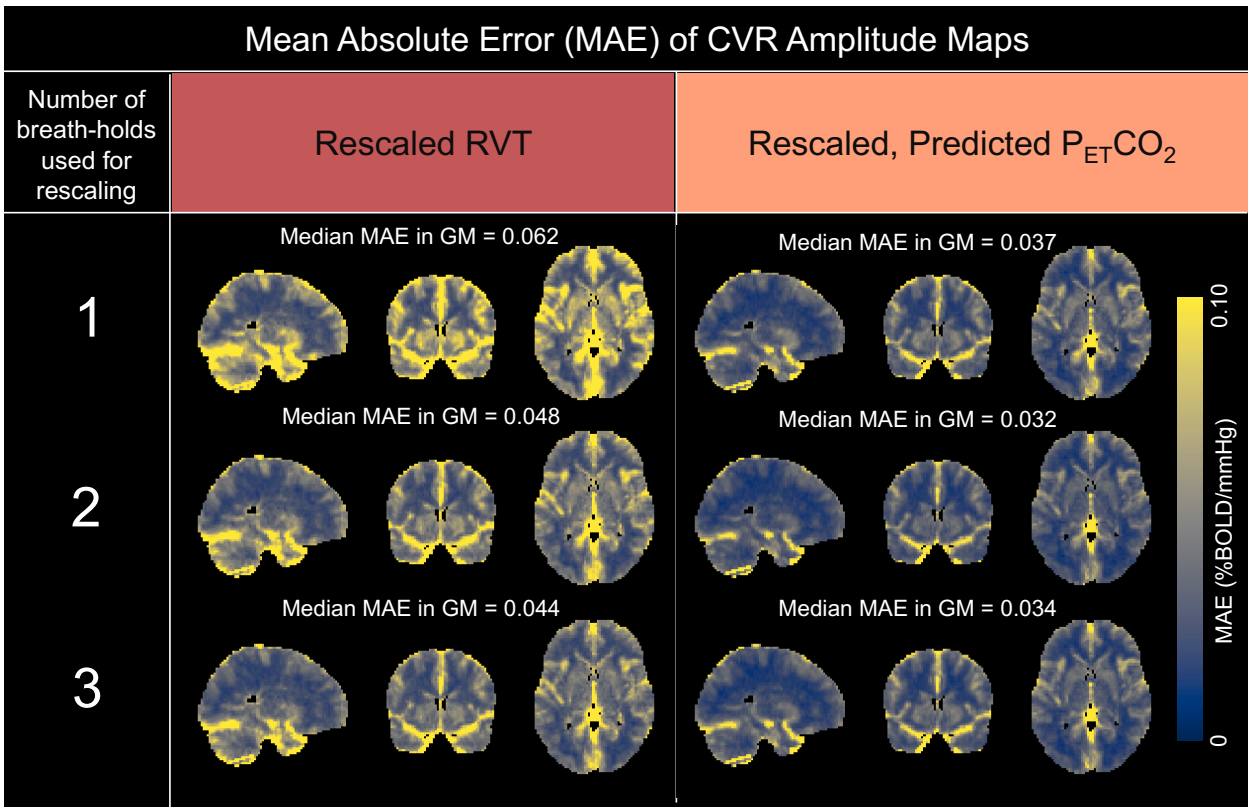

Figure 8. MAE maps comparing amplitude values generated using rescaled RVT and rescaled, predicted $P_{ET}CO_2$ to the ground truth amplitude values generated using measured $P_{ET}CO_2$. Maps are shown for each of the 3 different rescaling methods. The median MAE in gray matter (%BOLD/mmHg) is shown above each map.

In terms of CVR delay, which is not sensitive to rescaling, the predicted $P_{ET}CO_2$ method outperformed the RVT method, with a median absolute difference in gray matter of 0.97 seconds compared to 1.51 seconds (Figure 9). Again, the errors for both maps appear relatively consistent throughout gray matter.

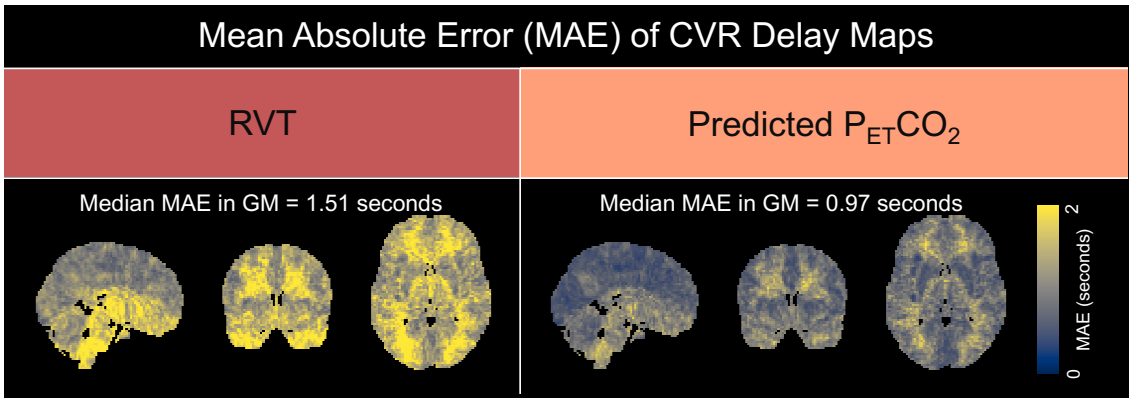

Figure 9. MAE maps comparing delay values generated using rescaled RVT and rescaled, predicted $P_{ET}CO_2$ to the ground truth delay values generated using measured $P_{ET}CO_2$. The median absolute difference in gray matter (%BOLD/mmHg) is shown above each map.

At the scan level, we also evaluated the distribution of the median absolute errors of CVR amplitude in gray matter relative to the ground truth amplitude maps for each regressor and rescaling method (Figure 10). When rescaling was performed using 1 or 2 breath holds, the amplitude errors for predicted $P_{ET}CO_2$ were significantly lower than the errors for RVT. When rescaling was performed using 3 breath holds, the amplitude errors for predicted $P_{ET}CO_2$ were not significantly different than the errors for RVT. For rescaling RVT, using 2 breath hold compared to 1 resulted in significantly decreased errors (p<0.05, Bonferroni corrected), but 3 breath holds compared to 2 did not significantly change the errors. On the other hand, for rescaling predicted $P_{ET}CO_2$, using 2 breath holds compared to 1 did not significantly change the distribution of errors, but using 3 breath holds compared to 2 significantly increased errors (p<0.05, Bonferroni corrected).

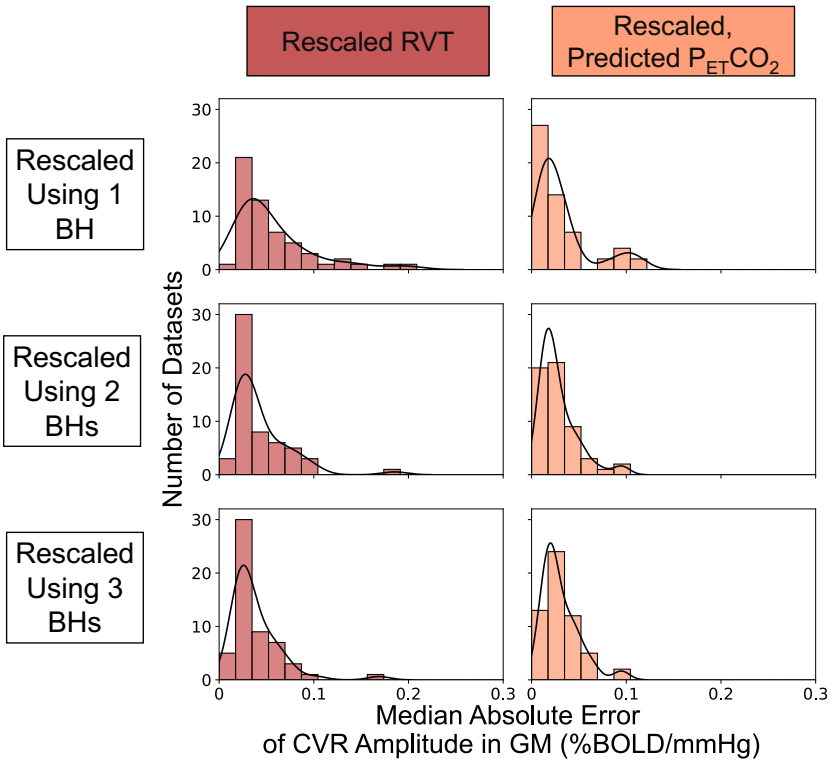

Figure 10. Distributions of the median absolute errors of CVR amplitude in gray matter (GM) across scans. Results are shown for CVR amplitude values generated using RVT and

predicted $P_{ET}CO_2$ regressors rescaled using 1, 2, and 3 breath holds (BHs). For each distribution, the kernel density estimate is overlaid to aid in visualization.

Lastly, we calculated Spearman rank correlations to evaluate whether the RVT and predicted $P_{ET}CO_2$ regressors preserve the ranking of median CVR amplitude values in gray matter across scans (Table 2). All 3 rescaling methods resulted in a significant correlation between the rankings of CVR amplitude values derived from both regressors and the ground truth amplitude rankings. For both predicted $P_{ET}CO_2$ and RVT, using more breath holds for rescaling increased the Spearman rank correlation with the ground truth amplitude values. However, across the 3 rescaling methods, the amplitude rankings from rescaled, predicted $P_{ET}CO_2$ showed a higher Spearman correlation with the ground truth amplitude rankings than those from rescaled RVT.

Table 2. Spearman's rank correlations comparing the median CVR amplitudes in gray matter generated using measured $P_{ET}CO_2$ to those generated using RVT and predicted $P_{ET}CO_2$ for each of the 3 rescaling methods. Asterisks indicate significant correlations (p<0.05).

	Spearman's Rank Correlation	
Number of breath-holds used for rescaling	Measured $P_{ET}CO_2$ Amplitudes and Rescaled RVT Amplitudes	Measured $P_{ET}CO_2$ Amplitudes and Rescaled Predicted $P_{ET}CO_2$ Amplitudes
1	0.73*	0.78*
2	0.81*	0.89*
3	0.83*	0.91*

3.5. CVR amplitude and delay maps for scans with low-quality breath holds

Next, we evaluated the utility of using a rescaled RVT or rescaled, predicted $P_{ET}CO_2$ regressor to map CVR in 2 scans with measured $P_{ET}CO_2$ regressors containing mostly low-quality breath holds (Figure 11). As anticipated, the amplitude maps generated using measured $P_{ET}CO_2$ timeseries lack the expected contrast between gray and white matter. They also do not appear spatially similar to a reference CVR map for the same subject from a different session with superior $P_{ET}CO_2$ quality. In comparison, the maps generated using rescaled RVT and rescaled, predicted $P_{ET}CO_2$ regressors appear more spatially similar to the reference maps, which is supported by their higher spatial correlations in gray matter to the

reference maps. This suggests that rescaled RVT and rescaled, predicted $P_{ET}CO_2$ regressors can be used to recover reasonable maps of CVR amplitude and delay. However, while the CVR amplitude maps generated using rescaled RVT and predicted $P_{ET}CO_2$ appear relatively similar, the delay maps generated using predicted $P_{ET}CO_2$ consistently have a higher spatial correlation to the reference map than the delay maps generated using RVT.

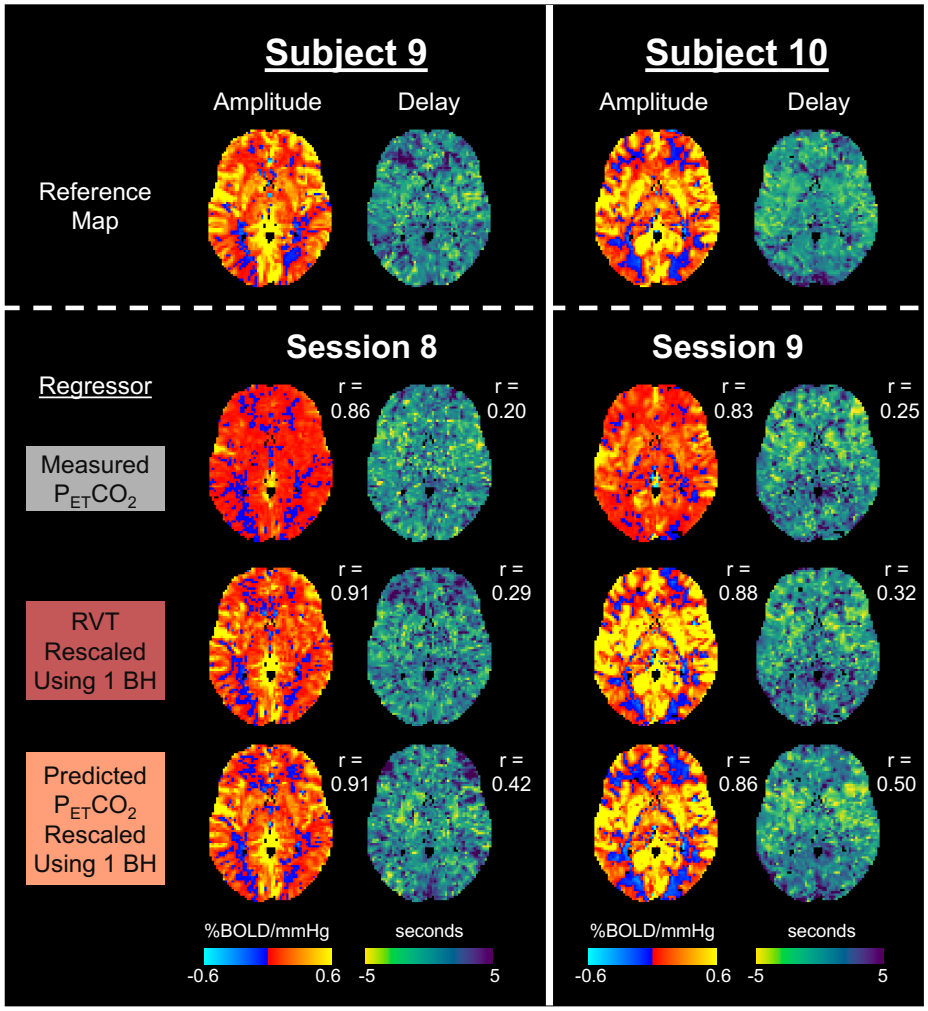

Figure 11. CVR amplitude and delay maps for 2 scan sessions with measured $P_{ET}CO_2$ timeseries containing mostly low-quality breath holds. Reference CVR amplitude and delay maps, generated using high-quality data from the same subject for a different session, are provided to assess the accuracy of maps generated using the measured $P_{ET}CO_2$ regressor, rescaled RVT regressor, and rescaled, predicted $P_{ET}CO_2$ regressor. Spatial correlations in gray matter to the reference map (r) are provided.

3.6. Case study in a participant with Moyamoya disease

Lastly, we assessed the clinical utility of rescaled RVT and rescaled, predicted $P_{ET}CO_2$ regressors for mapping CVR amplitude and delay in a participant with unilateral Moyamoya disease affecting the right MCA territory. For this participant, each breath hold caused clear CO_2 changes (average change = 6.47 mmHg) and thus we could use the CVR amplitude and delay maps generated using the measured $P_{ET}CO_2$ trace as a reasonable ground truth. The first breath hold caused a CO_2 increase of 6.37 mmHg and was used for rescaling the RVT and predicted $P_{ET}CO_2$ regressors. As shown in Figure 12, the ground truth CVR amplitude map does not appear to be significantly impacted by pathology. Compared to the ground truth map, the CVR amplitude map generated using rescaled RVT shows more negative CVR values in the right hemisphere, particularly in the right MCA territory. In contrast, the amplitude map generated using rescaled, predicted $P_{ET}CO_2$ appears more similar to the ground truth map, which is supported by its higher spatial correlation in gray matter. The ground truth delay map shows that many voxels in the right hemisphere responded significantly later than voxels in the left hemisphere. Again, the delay map generated using rescaled, predicted $P_{ET}CO_2$ has a higher spatial correlation to the ground truth delay map than the rescaled RVT delay map. Our finding that CVR delay, but not amplitude, is primarily impacted by Moyamoya pathology in the ground truth maps agrees with previously reported results from a different scan of the same participant (Stickland et al., 2021).

To better understand whether RVT and predicted $P_{ET}CO_2$ regressors can be used to identify regions of extreme delay values, we thresholded the delay maps to isolate binary clusters with delay values greater than 10 seconds. The Dice similarity coefficient of clusters in the RVT and measured $P_{ET}CO_2$ delay maps was 0.16, while it was 0.66 for the clusters in predicted and measured $P_{ET}CO_2$ delay maps. This indicates that the CVR delay map generated using predicted $P_{ET}CO_2$ is more successful than RVT at characterizing this regional pathology.

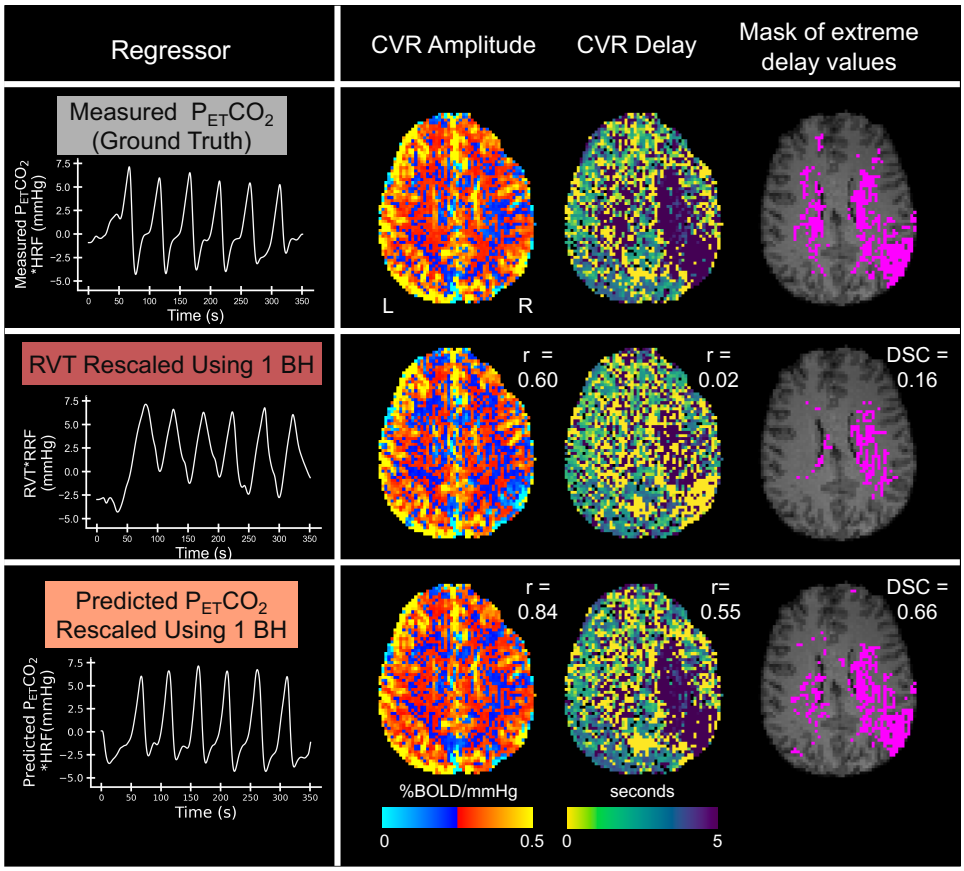

Figure 12. Maps of CVR amplitude, CVR delay, and extreme delay values for a participant with unilateral Moyamoya disease affecting the right middle cerebral artery. Maps were generated using 3 different regressors (from top to bottom): measured $P_{ET}CO_2$, rescaled RVT, and rescaled, predicted $P_{ET}CO_2$. For the amplitude and delay maps, spatial correlations (r) to the measured $P_{ET}CO_2$ (ground truth) map in gray matter are provided. For each mask of extreme delay values, the Dice similarity coefficient (DSC) to the mask generated from the measured $P_{ET}CO_2$ delay map is provided.

4. Discussion

Obtaining accurate $P_{ET}CO_2$ data is challenging, particularly in clinical populations, which limits our ability to accurately map CVR. In this work, we explored computational methods for improving $P_{ET}CO_2$ data quality while maintaining units of mmHg to allow for CVR to be mapped in standard units (%BOLD/mmHg). Since we observed that most participants can complete at least 1 high-quality breath-hold trial, our approach focused on leveraging high-quality measured $P_{ET}CO_2$ data from one or more trials to rescale two alternative regressors that reflect relative changes in $P_{ET}CO_2$ to mmHg. First, we investigated mapping CVR using a rescaled RVT regressor, which reflects changes in breathing rate and depth that cause

changes in arterial CO_2. RVT is a more feasible measure than $P_{ET}CO_2$ since it does not require additional task compliance from participants, but it is non-quantitative (i.e., recorded in arbitrary units). To try to better model the shape of the BOLD response to a change in arterial CO_2 and more accurately map CVR, we also investigated whether we could predict z-normalized $P_{ET}CO_2$ from RVT using deep learning and rescale the predicted $P_{ET}CO_2$ timeseries to mmHg. Our results suggest that both rescaled RVT and rescaled, predicted $P_{ET}CO_2$ can be used to recover reasonable maps of CVR amplitude and delay. However, the rescaled, predicted $P_{ET}CO_2$ regressor is more accurate and may be more appropriate for mapping CVR in clinical populations.

4.1. Task compliance trends

To train and validate our $P_{ET}CO_2$ prediction model, we used a dataset consisting of 245 exhaled CO_2 and respiration effort timeseries simultaneously recorded during a breath-hold task. To evaluate RVT and predicted $P_{ET}CO_2$ for mapping CVR, we used the publicly available EuskalIBUR dataset, consisting of fMRI data, exhaled CO_2 timeseries, and respiration effort timeseries simultaneously recorded during a breath-hold task for 99 total scans across 10 participants. Leveraging the large sizes of these datasets, we explored general trends in breath-hold task compliance in healthy participants. In both datasets, we found that nearly half of the CO_2 recordings contained at least 1 low-quality breath-hold trial (Figure 3), indicating that CVR accuracy could be compromised in at least half of the cases. In participants with neurological diseases and in children, even lower task compliance is expected (Schlund et al., 2011; Spano et al., 2013). These results underscore the importance of developing alternative methods for mapping CVR in standard units when $P_{ET}CO_2$ quality is low in order to allow for CVR comparisons across subjects and scan sessions. Additionally, we found that only 4.5% and 7% of CO_2 recordings in the training and EuskalIBUR datasets, respectively, did not contain any high-quality breath-hold trials (Figure 3). This finding demonstrates the overall feasibility of breath-hold tasks; while imperfect task compliance is common, only a small percentage of recordings were completely unusable. Importantly, this finding also suggests that rescaling using 1 high-quality breath hold is feasible in the vast majority of CO_2 recordings; with coaching and real time feedback, we expect that even more recordings could contain at least 1 high-quality breath hold.

4.2. Accuracy of $P_{ET}CO_2$ prediction

We trained a 1D FCN to predict $P_{ET}CO_2$ from RVT and, prior to convolution with the HRF, achieved a mean Fisher's z-transformed correlation of 1.14 ± 0.3 with measured $P_{ET}CO_2$ on our held-out test set. Previously described results in the literature focused on predicting CO_2 from respiration recordings in *resting-state* data and deriving $P_{ET}CO_2$ from the predicted CO_2 timeseries (Agrawal et al., 2023); the authors achieved a mean Pearson correlation of 0.512 ± 0.3 to measured $P_{ET}CO_2$. For comparison to these results and to assess the benefits of using breath-hold instead of resting-state data, we calculated the mean Pearson correlation (not normalized to Fisher's z) of measured and predicted $P_{ET}CO_2$ in the EuskalIBUR dataset and found that our model achieved a value of 0.787 ± 0.1. Ultimately, this high correlation supports our hypothesis that since breath holds cause large fluctuations in CO_2, using breath-hold data may allow for more robust prediction of $P_{ET}CO_2$ than can be achieved with resting-state data.

Additionally, when we evaluated our regressors using the EuskalIBUR dataset, we found that regardless of the rescaling method used, the predicted $P_{ET}CO_2$ timeseries had higher normalized correlations and lower MAEs and MSEs to measured $P_{ET}CO_2$ than RVT (Figure 5). This suggests that the FCN model effectively identified patterns between RVT and $P_{ET}CO_2$ changes, and that the predicted $P_{ET}CO_2$ regressor provides additional information about relative $P_{ET}CO_2$ changes beyond what RVT alone can provide.

4.3. Observations and suggestions related to rescaling $P_{ET}CO_2$ and RVT to mmHg

To better understand how many high-quality breath holds are required for accurate rescaling to units of mmHg, we assessed the error of predicted $P_{ET}CO_2$ and RVT regressors rescaled using 1, 2, and 3 breath holds relative to measured $P_{ET}CO_2$ (Figure 5). Rescaling using more breath holds did not significantly change any measures of error for both predicted $P_{ET}CO_2$ and RVT, except that rescaling predicted $P_{ET}CO_2$ using 2 breath holds compared to 1 breath hold significantly decreased the MAE.

In addition to investigating whether using more breath holds for rescaling impacted the accuracy of the regressor, we also investigated how using more breath holds for rescaling impacted the actual CVR amplitude estimates (note that CVR delay is not sensitive to rescaling). By assessing the distribution of the median absolute error in gray matter for CVR amplitude values calculated using RVT (Figure 10), we found that using 2 breath holds for rescaling may be optimal (i.e., result in lower errors of CVR amplitude in gray matter) for RVT. For rescaling predicted $P_{ET}CO_2$, using more breath holds did not significantly decrease the median absolute error in gray matter. We also assessed how well the rescaled, predicted

$P_{ET}CO_2$ and rescaled RVT regressors preserved the relative rankings of CVR amplitudes in gray matter across subjects, and found that using more breath holds for rescaling made the relative CVR rankings more correlated with the ground truth rankings (Table 2).

We suggest that while using more breath holds for rescaling RVT or predicted $P_{ET}CO_2$ may improve CVR accuracy, rescaling using 1 breath hold is sufficient. To support this, we showed that CVR amplitude and delay maps generated using RVT or predicted $P_{ET}CO_2$ rescaled using 1 breath hold appear highly similar to ground truth maps (Figures 6 and 7). We also provided examples from 2 scans with low-quality measured $P_{ET}CO_2$ timeseries that showed that reasonable maps of CVR amplitude and delay can be recovered using RVT or predicted $P_{ET}CO_2$ when only 1 breath hold is used for rescaling (Figure 11). Additionally, in our case study on a participant with Moyamoya disease, we showed that when 1 breath hold is used for rescaling, predicted $P_{ET}CO_2$ produces CVR amplitude and delay maps that are highly similar to the ground truth maps and sensitive to cerebrovascular pathology (Figure 12).

Another important consideration when rescaling predicted $P_{ET}CO_2$ or RVT regressors is defining a threshold for a high-quality breath hold. We defined this threshold by calculating the average breath hold increase minus 1 standard deviation across all of the breath holds in the dataset that caused a positive CO_2 change. For the EuskalIBUR dataset, the mean CO_2 increase across all breath holds causing a CO_2 increase was 6.73 mmHg (mean increase – 1 standard deviation = 3.60 mmHg), and for the training dataset collected in our lab environment, the mean CO_2 increase was 9.85 mmHg (mean increase – 1 standard deviation = 6.33 mmHg). It is surprising that the average CO_2 increase in the training dataset was so much larger. Previously, average CO_2 increases of approximately 9 mmHg (Tancredi & Hoge, 2013) and 13.4 mmHg (Murphy et al., 2011) in response to 20 second breath holds have been reported in healthy participants. This discrepancy could be related to sampling line lengths and vacuum settings resulting in dispersion of the exhaled gases and more mixing with room air, reducing the perceived CO_2 changes. At minimum, a threshold of 3.60 mmHg should be used for a 20 second breath hold to be considered high-quality; however, using a more stringent threshold may result in more accurate rescaling of predicted $P_{ET}CO_2$ or RVT regressors. Future work should focus on establishing guidelines for classifying breath holds as high-quality that are unique to the length of the breath hold, patient population, and perhaps even the individual participant.

To ensure that at least one high-quality breath hold is collected, we recommend that researchers monitor the change in exhaled CO_2 levels induced by each breath-hold during the scan. Developing a real-time feedback tool that could automatically output whether a

recently completed breath hold was high-quality would be particularly beneficial for this monitoring. If the participant does not achieve any high-quality breath holds during the task and scan time allows, researchers could ask the participants to perform additional trials.

4.4. Which is better: rescaled RVT or rescaled, predicted $P_{ET}CO_2$?

Our findings suggest that the rescaled, predicted $P_{ET}CO_2$ regressor produces more accurate maps of CVR amplitude and delay than rescaled RVT. Group-level MAE maps for CVR amplitude estimations showed that, across the 3 rescaling methods, predicted $P_{ET}CO_2$ consistently had a lower median MAE in gray matter compared to RVT (Figure 8). Additionally, group-level MAE maps for CVR delay showed that the predicted $P_{ET}CO_2$ regressor outperformed the RVT regressor, with a median MAE of 0.97 compared to 1.51 seconds (Figure 9). When we looked at the distribution of median absolute errors in gray matter for CVR amplitude across scans (Figure 10), we found that when rescaling was performed using 1 or 2 breath-holds, predicted $P_{ET}CO_2$ had significantly lower median absolute errors in gray matter compared to RVT. Additionally, we found that across all 3 rescaling methods, predicted $P_{ET}CO_2$ better preserves the rankings of median CVR amplitudes in gray matter across scans than RVT (Table 2).

Our case study on a participant with unilateral Moyamoya disease (Figure 12) highlights the superior performance of rescaled, predicted $P_{ET}CO_2$ for estimating CVR amplitude and delay and suggests that the predicted $P_{ET}CO_2$ regressor may provide the necessary sensitivity to detect impairments in CVR delay. Increased blood flow delays have been commonly reported in Moyamoya disease, which causes narrowing of cerebral blood vessels (Donahue et al., 2015; S. K. Kim et al., 2003; Stickland et al., 2021). In line with previous findings (Stickland et al., 2021), we found that the ground truth CVR amplitude map was relatively unaffected by Moyamoya disease, while the ground truth delay map showed increased delays in the right hemisphere, particularly in the vascular territory of the right middle cerebral artery, which is affected by Moyamoya disease. The amplitude and delay maps generated using rescaled, predicted $P_{ET}CO_2$ had higher spatial correlations to the ground truth maps than the maps generated using rescaled RVT. In particular, the delay map generated using predicted $P_{ET}CO_2$ was better able to identify the region of extreme delay values compared to the RVT map.

More extensive research is needed to determine whether the level of accuracy associated with the rescaled, predicted $P_{ET}CO_2$ regressor is sufficient to identify meaningful differences in CVR amplitude across various populations. When 1 breath-hold was used for rescaling,

predicted $P_{ET}CO_2$ produced a median MAE in gray matter of 0.037 %BOLD/mmHg (Figure 8). This error is smaller than some previously reported CVR differences across populations; for example, gray matter CVR amplitude differences of 0.07 %BOLD/mmHg between young and elderly subjects have been reported (Bhogal et al., 2016). In participants with small vessel disease and traumatic brain injury, CVR amplitude differences relative to controls of 0.062-0.079 %BOLD/mmHg and 0.042 %BOLD/mmHg, respectively, have been reported (Thrippleton et al., 2018; Bhogal et al., 2016).

4.5. Generalizability of $P_{ET}CO_2$ prediction model

To predict $P_{ET}CO_2$ from RVT, we trained and validated our model using a dataset collected in our lab environment, and then tested the model using the publicly available EuskalIBUR dataset. One benefit of this approach is that it shows our model is generalizable to data collected in other research environments; however, additional work could be done to further increase the generalizability of our model. For example, to mimic participants failing to perform the trial, we collected 55 datasets in which, for each of the 10 breath holds, there was a 10% chance that the breath hold would be skipped and replaced with a period of rest. However, these 55 datasets are only a small portion of our training dataset, and our model could be improved by adding more skipped breath holds to the training dataset. With more datasets containing skipped breath holds, we could also specifically evaluate how the model predicts $P_{ET}CO_2$ when a breath hold is skipped. Additionally, our in-house training dataset and the EuskalIBUR testing dataset consisted of mostly participants in their 20s and 30s; future work could focus on collecting data in a wider age range of participants to make the model more generalizable to the broader population. Additionally, conditions such as chronic obstructive pulmonary disease and pulmonary hypertension may cause atypical relationships between ventilation (and RVT) and arterial CO_2 and should be specifically incorporated into future model improvements (Reybrouck et al., 1998; Teopompi et al., 2013).

4.6. Suggestions for implementing breath-hold fMRI for CVR mapping

To increase the likelihood that participants will successfully complete the breath-hold task, we strongly recommend allotting time before the scan for participants to practice the task. In particular, we recommend having the participant wear the nasal cannula and practice exhaling after each breath hold so that the researcher can check that the expected increase in CO_2 is being measured and provide feedback if needed. Additionally, real-time monitoring of exhaled CO_2 *or* the respiratory belt during the scan is critical for assessing whether participants are

even attempting the breath-hold task, distinct from whether the end-tidal information is successfully captured. An important caveat of using alternative regressors like RVT or predicted $P_{ET}CO_2$ to map CVR is that they require the participant to have attempted the breath-hold task; this means that even if the participant didn't exhale immediately after the breath hold or accidentally breathed through their mouth, they still held their breath for most of the breath-hold periods in the task. If the participant does not seem to be attempting the breath holds at all, the researcher should stop the task and check on the participant, and, time permitting, ask the participant to redo the task.

Another important consideration is that, while respiratory belt measurements do not necessitate additional task compliance for accuracy—making them more feasible than $P_{ET}CO_2$ measurements—careful setup is required to properly measure respiration and ensure accurate RVT measurements. In particular, it is critical to ensure that the belt is not too loose or too tight to avoid signal saturation, which is more common in particularly large or small participants. Before the scan starts, we recommend instructing participants to take a deep breath in and out while monitoring the resulting signals. If the signals appear saturated, it is an indication that the tightness of the respiratory belt should be adjusted.

Our lab is currently adapting existing real-time analysis tools, originally used to give visual feedback for force targeting during motor-task fMRI (Reddy et al., 2024) to provide researchers with ongoing insight into breath-hold trial performance and signal quality during scanning. We anticipate that this approach will ensure that CVR is successfully mapped in the majority of clinical research subjects, using an efficient protocol that focuses on sufficient data quality for each individual instead of a one-size-fits-all acquisition approach.

4.7. Future work

In this study, we used a 1D FCN to predict $P_{ET}CO_2$ from RVT, which is a relatively simple, computationally efficient approach. Due to our limited training dataset size, our FCN used a discrete stopping criterion based on a fixed number of epochs. Future work will focus on integrating early stopping techniques to enhance model reliability and robustness and mitigate overfitting. In the future, other types of models could also be investigated for predicting $P_{ET}CO_2$ when measured $P_{ET}CO_2$ quality is low. One alternative approach is using a time series forecasting model to predict low-quality segments of a $P_{ET}CO_2$ timeseries from high-quality segments earlier in the timeseries. In this approach, the RVT timeseries could be included as a covariate. By focusing on forecasting a part of the $P_{ET}CO_2$ timeseries rather than predicting the entire time series, this approach may allow the $P_{ET}CO_2$ predictions to be in mmHg,

eliminating the need for an additional rescaling step. Another alternative model is a U-Net, which incorporates skip connections to prevent the vanishing gradients problem and has been used to successfully predict respiratory volume fluctuations from fMRI data (Bayrak et al., 2020).

Additionally, while we showed that the predicted $P_{ET}CO_2$ method can be used to identify brain regions of extreme CVR delays in a single case study of an individual with unilateral Moyamoya disease, more extensive validation is needed to establish the sensitivity of the CVR amplitude and delay maps generated using rescaled, predicted $P_{ET}CO_2$ and rescaled RVT regressors to cerebrovascular pathology. Specifically, investigation in participants with CVR amplitude maps affected by cerebrovascular pathology is required, since CVR delay, rather than amplitude, was primarily affected in the participant with Moyamoya disease. Our ongoing research efforts include applying our methodology in participants with sub-acute and chronic stroke, to evaluate if RVT or predicted $P_{ET}CO_2$ remains suitable for delineating the pathological hemodynamics expected in this cohort (Krainik et al., 2005; Siegel et al., 2016).

5. Conclusions

We demonstrated that either an RVT or $P_{ET}CO_2$ regressor predicted from RVT can be rescaled using high-quality $P_{ET}CO_2$ data for at least one breath hold and used to model both the amplitude and delay of the CVR response to a breath-hold task. The predicted $P_{ET}CO_2$ regressor produces more accurate CVR amplitude and delay maps and may provide greater sensitivity to cerebrovascular pathologies. Importantly, our method (using either model) allows for CVR amplitude to be modeled in standard units (%BOLD/mmHg), facilitating CVR comparisons across subjects and scan sessions and the establishment of normative ranges of healthy CVR values. Ultimately, this work will increase the feasibility of CVR mapping in clinical settings where breath-hold task compliance may be variable.

Data and Code Availability

Physiological data used for model training is available on OSF at https://doi.org/10.17605/OSF.IO/Y5CK4 (Clements et al., 2024). The EuskalIBUR dataset is available on OpenNeuro at doi:10.18112/openneuro.ds003192.v1.0.1 (Moia, Uruñuela, Ferrer, & Caballero-Gaudes, 2020). MRI pre-processing code is available at https://github.com/BrightLab-ANVIL/PreProc_BRAIN. Phys2cvr (Moia, Vigotsky, & Zvolanek, 2022), a publicly available Python tool, was used for computing CVR amplitude and delay maps. Additional analysis code is available at https://github.com/BrightLab-ANVIL/Clements_BHCVR-PredictedCO2.

Author Contributions

Rebecca G. Clements: Conceptualization, Methodology, Software, Formal analysis, Investigation, Data curation, Writing – original draft, Writing – reviewing and editing, Visualization, Project administration. **Kristina M. Zvolanek:** Conceptualization, Methodology, Writing – reviewing and editing. **Neha A. Reddy:** Methodology, Writing – reviewing and editing. **Kimberly J. Hemmerling:** Formal Analysis, Writing – reviewing and editing. **Roza G. Bayrak:** Methodology, Writing – reviewing and editing. **Catie Chang:** Methodology, Writing – reviewing and editing. **Molly G. Bright:** Conceptualization, Methodology, Resources, Writing – review & editing, Supervision, Project administration, Funding acquisition.

Funding

This work was supported by the National Science Foundation (DGE-2234667 to R.G.C.) and the National Institutes of Health (T32EB025766 to K.M.Z., N.A.R., and K.J.H., F31HL166079 to K.M.Z., and F31NS134222 to K.J.H.).

Declaration of Competing Interests

The authors declare no competing financial interests.

Acknowledgements

The authors would like to thank Chris Chin, Katie Friedman, Sara Hudson, Robbie Ng, and Kelly Tichenor in the Northwestern University Department of Physical Therapy and Human Movement Sciences for their contributions to data collection. In addition, this research was supported in part through the computational resources and staff contributions provided for the Quest high performance computing facility at Northwestern University which is jointly supported by the Office of the Provost, the Office for Research, and Northwestern University Information Technology. This research was also supported by the Center for Translational Imaging at Northwestern University.

References

Agrawal, V., Zhong, X. Z., & Chen, J. J. (2023). Generating dynamic carbon-dioxide traces from respiration-belt recordings: Feasibility using neural networks and application in functional magnetic resonance imaging. *Frontiers in Neuroimaging*, *2*, 1119539. https://doi.org/10.3389/FNIMG.2023.1119539

Bayrak, R. G., Salas, J. A., Huo, Y., & Chang, C. (2020). A Deep Pattern Recognition Approach for Inferring Respiratory Volume Fluctuations from fMRI Data. *International Conference on Medical Image Computing and Computer-Assisted Intervention, 12267*, 428–436. https://doi.org/10.1007/978-3-030-59728-3_42

Bhogal, A. A., De Vis, J. B., Siero, J. C. W., Petersen, E. T., Luijten, P. R., Hendrikse, J., Philippens, M. E. P., & Hoogduin, H. (2016). The BOLD cerebrovascular reactivity response to progressive hypercapnia in young and elderly. *NeuroImage*, *139*, 94–102. https://doi.org/10.1016/J.NEUROIMAGE.2016.06.010

Birn, R. M., Diamond, J. B., Smith, M. A., & Bandettini, P. A. (2006). Separating respiratory-variation-related fluctuations from neuronal-activity-related fluctuations in fMRI. *NeuroImage*, *31*(4), 1536–1548. https://doi.org/10.1016/J.NEUROIMAGE.2006.02.048

Birn, R. M., Smith, M. A., Jones, T. B., & Bandettini, P. A. (2008). The respiration response function: The temporal dynamics of fMRI signal fluctuations related to changes in respiration. *NeuroImage*, *40*(2), 644–654. https://doi.org/10.1016/J.NEUROIMAGE.2007.11.059

Bright, M. G., & Murphy, K. (2013). Reliable quantification of BOLD fMRI cerebrovascular reactivity despite poor breath-hold performance. *NeuroImage*, *83*, 559–568. https://doi.org/10.1016/J.NEUROIMAGE.2013.07.007

Chang, C., & Glover, G. H. (2009). Relationship between respiration, end-tidal CO2, and BOLD signals in resting-state fMRI. *NeuroImage*, *47*(4), 1381. https://doi.org/10.1016/J.NEUROIMAGE.2009.04.048

Chiarelli, A. M., Villani, A., Mascali, D., Petsas, N., Biondetti, E., Caporale, A., Digiovanni, A., Grasso, E. A., Ajdinaj, P., D'Apolito, M., Rispoli, M. G., Sensi, S., Murphy, K., Pozzilli, C., Wise, R. G., & Tomassini, V. (2022). Cerebrovascular reactivity in multiple sclerosis is restored with reduced inflammation during immunomodulation. *Scientific Reports 2022 12:1*, *12*(1), 1–11. https://doi.org/10.1038/s41598-022-19113-8

Clements, R., Hemmerling, K. J., Reddy, N., Zvolanek, K., & Bright, M. (2024). Quantitative mapping of cerebrovascular reactivity amplitude and delay with breath-hold BOLD fMRI when end-tidal CO2 quality is low. *OSF*. [Dataset] https://doi.org/10.17605/OSF.IO/Y5CK4

Cox, R. W. (1996). AFNI: Software for Analysis and Visualization of Functional Magnetic Resonance Neuroimages. *Computers and Biomedical Research*, *29*(3), 162–173. https://doi.org/10.1006/CBMR.1996.0014

Crosby, A., & Robbins, P. A. (2004). Variability in end-tidal PCO2 and blood gas values in humans. *Experimental Physiology*, *88*(5), 603–610. https://doi.org/10.1113/eph8802585

Davis, T. L., Kwong, K. K., Weisskoff, R. M., & Rosen, B. R. (1998). Calibrated functional MRI: Mapping the dynamics of oxidative metabolism. *Proceedings of the National Academy of Sciences of the United States of America*, *95*(4), 1834–1839. https://doi.org/10.1073/PNAS.95.4.1834/ASSET/7B6AC16D-B019-49E8-9909-63BD75C34ECF/ASSETS/GRAPHIC/PQ0384059004.JPEG

De Vis, J. B., Bhogal, A. A., Hendrikse, J., Petersen, E. T., & Siero, J. C. W. (2018). Effect sizes of BOLD CVR, resting-state signal fluctuations and time delay measures for the assessment of hemodynamic impairment in carotid occlusion patients. *NeuroImage*, *179*, 530–539. https://doi.org/10.1016/J.NEUROIMAGE.2018.06.017

Donahue, M. J., Strother, M. K., Lindsey, K. P., Hocke, L. M., Tong, Y., & Frederick, B. D. (2015). Time delay processing of hypercapnic fMRI allows quantitative parameterization of cerebrovascular reactivity and blood flow delays. *Journal of Cerebral Blood Flow and Metabolism*, *36*(10). https://doi.org/10.1177/0271678X15608643

DuPre, E., Salo, T., Ahmed, Z., Bandettini, P. A., Bottenhorn, K. L., Caballero-Gaudes, C., Dowdle, L. T., Gonzalez-Castillo, J., Heunis, S., Kundu, P., Laird, A. R., Markello, R., Markiewicz, C. J., Moia, S., Staden, I., Teves, J. B., Uruñuela, E., Vaziri-Pashkam, M., Whitaker, K., & Handwerker, D. A. (2021). TE-dependent analysis of multi-echo fMRI with *tedana*. *Journal of Open Source Software*, *6*(66), 3669. https://doi.org/10.21105/JOSS.03669

Friston, K. J., Fletcher, P., Josephs, O., Holmes, A., Rugg, M. D., & Turner, R. (1998). Event-Related fMRI: Characterizing Differential Responses. *NeuroImage*, *7*(1), 30–40. https://doi.org/10.1006/NIMG.1997.0306

Golestani, A. M., Chang, C., Kwinta, J. B., Khatamian, Y. B., & Jean Chen, J. (2015). Mapping the end-tidal CO2 response function in the resting-state BOLD fMRI signal: Spatial specificity, test–retest reliability and effect of fMRI sampling rate. *NeuroImage*, *104*, 266–277. https://doi.org/10.1016/J.NEUROIMAGE.2014.10.031

Golestani, A. M., Wei, L. L., & Chen, J. J. (2016). Quantitative mapping of cerebrovascular reactivity using resting-state BOLD fMRI: Validation in healthy adults. *NeuroImage*, *138*, 147–163. https://doi.org/10.1016/J.NEUROIMAGE.2016.05.025

Handwerker, D. A., Ollinger, J. M., & D'Esposito, M. (2004). Variation of BOLD hemodynamic responses across subjects and brain regions and their effects on statistical analyses. *NeuroImage*, *21*(4), 1639–1651. https://doi.org/10.1016/J.NEUROIMAGE.2003.11.029

Jenkinson, M., Beckmann, C. F., Behrens, T. E. J., Woolrich, M. W., & Smith, S. M. (2012). FSL. *NeuroImage*, *62*(2), 782–790. https://doi.org/10.1016/J.NEUROIMAGE.2011.09.015

Kastrup, A., Krüger, G., Neumann-Haefelin, T., & Moseley, M. E. (2001). Assessment of cerebrovascular reactivity with functional magnetic resonance imaging: comparison of CO2 and breath holding. *Magnetic Resonance Imaging*, *19*(1), 13–20. https://doi.org/10.1016/S0730-725X(01)00227-2

Kim, D., Hughes, T. M., Lipford, M. E., Craft, S., Baker, L. D., Lockhart, S. N., Whitlow, C. T., Okonmah-Obazee, S. E., Hugenschmidt, C. E., Bobinski, M., & Jung, Y. (2021). Relationship Between Cerebrovascular Reactivity and Cognition Among People With Risk of Cognitive Decline. *Frontiers in Physiology*, *12*, 645342. https://doi.org/10.3389/FPHYS.2021.645342/BIBTEX

Kim, S. K., Wang, K. C., Oh, C. W., Kim, I. O., Lee, D. S., Song, I. C., & Cho, B. K. (2003). Evaluation of Cerebral Hemodynamics with Perfusion MRI in Childhood Moyamoya Disease. *Pediatric Neurosurgery*, *38*(2), 68–75. https://doi.org/10.1159/000068050

Kingma, D. P., & Lei Ba, J. (2015). ADAM: A Method for Stochastic Optimization. *ICLR*.

Krainik, A., Hund-Georgiadis, M., Zysset, S., & Von Cramon, D. Y. (2005). Regional Impairment of Cerebrovascular Reactivity and BOLD Signal in Adults After Stroke. *Stroke*, *36*(6), 1146–1152. https://doi.org/10.1161/01.STR.0000166178.40973.A7

Kundu, P., Brenowitz, N. D., Voon, V., Worbe, Y., Vértes, P. E., Inati, S. J., Saad, Z. S., Bandettini, P. A., & Bullmore, E. T. (2013). Integrated strategy for improving functional connectivity mapping using multiecho fMRI. *Proceedings of the National Academy of Sciences of the United States of America*, *110*(40), 16187–16192. https://doi.org/10.1073/pnas.1301725110

Kundu, P., Inati, S. J., Evans, J. W., Luh, W. M., & Bandettini, P. A. (2012). Differentiating BOLD and non-BOLD signals in fMRI time series using multi-echo EPI. *NeuroImage*, *60*(3), 1759–1770. https://doi.org/10.1016/J.NEUROIMAGE.2011.12.028

Leung, J., Kim, J. A., & Kassner, A. (2016). Reproducibility of Cerebrovascular Reactivity Measures in Children Using BOLD MRI. *J. MAGN. RESON. IMAGING*, *43*, 1191–1195. https://doi.org/10.1002/jmri.25063

Liu, P., De Vis, J. B., & Lu, H. (2019). Cerebrovascular reactivity (CVR) MRI with CO2 challenge: A technical review. *NeuroImage*, *187*, 104–115. https://doi.org/10.1016/J.NEUROIMAGE.2018.03.047

Liu, P., Hebrank, A. C., Rodrigue, K. M., Kennedy, K. M., Section, J., Park, D. C., & Lu, H. (2013). Age-related differences in memory-encoding fMRI responses after accounting for decline in vascular reactivity. *NeuroImage*, *78*, 415–425. https://doi.org/10.1016/J.NEUROIMAGE.2013.04.053

Liu, P., Li, Y., Pinho, M., Park, D. C., Welch, B. G., & Lu, H. (2017). Cerebrovascular reactivity mapping without gas challenges. *NeuroImage*, *146*, 320–326. https://doi.org/10.1016/J.NEUROIMAGE.2016.11.054

Lu, H., Liu, P., Yezhuvath, U., Cheng, Y., Marshall, O., & Ge, Y. (2014). MRI Mapping of Cerebrovascular Reactivity via Gas Inhalation Challenges. *JoVE (Journal of Visualized Experiments)*, *94*, e52306. https://doi.org/10.3791/52306

Mathieu, F., Zeiler, F. A., Ercole, A., Monteiro, M., Kamnitsas, K., Glocker, B., Whitehouse, D. P., Das, T., Smielewski, P., Czosnyka, M., Hutchinson, P. J., Newcombe, V. F. J., & Menon, D. K. (2020). Relationship between Measures of Cerebrovascular Reactivity and Intracranial Lesion Progression in Acute Traumatic Brain Injury Patients: A CENTER-TBI Study. *Neurocritical Care, 37*(13), 1556–1565. https://doi.org/10.1089/NEU.2019.6814

Moia, S., Stickland, R. C., Ayyagari, A., Termenon, M., Caballero-Gaudes, C., & Bright, M. G. (2020a). Voxelwise optimization of hemodynamic lags to improve regional CVR estimates in breath-hold fMRI. *Proceedings of the Annual International Conference of the IEEE Engineering in Medicine and Biology Society, 2020-July*, 1489–1492. https://doi.org/10.1109/EMBC44109.2020.9176225

Moia, S., Termenon, M., Uruñuela, E., Chen, G., Stickland, R. C., Bright, M. G., & Caballero-Gaudes, C. (2021). ICA-based denoising strategies in breath-hold induced cerebrovascular reactivity mapping with multi echo BOLD fMRI. *NeuroImage*, *233*, 117914. https://doi.org/10.1016/J.NEUROIMAGE.2021.117914

Moia, S., Uruñuela, E., Ferrer, V., & Caballero-Gaudes, C. (2020b). *EuskalIBUR*. OpenNeuro. [Dataset] https://doi.org/10.18112/OPENNEURO.DS003192.V1.0.1

Moia, S., Vigotsky, A. D., & Zvolanek, K. M. (2024). *phys2cvr: A tool to compute Cerebrovascular Reactivity maps and associated lag maps*. https://doi.org/10.5281/ZENODO.7336002

Murphy, K., Harris, A. D., & Wise, R. G. (2011). Robustly measuring vascular reactivity differences with breath-hold: Normalising stimulus-evoked and resting state BOLD fMRI data. *NeuroImage*, *54*(1), 369–379. https://doi.org/10.1016/J.NEUROIMAGE.2010.07.059

Murrell, C. J., Cotter, J. D., Thomas, K. N., Lucas, S. J. E., Williams, M. J. A., & Ainslie, P. N. (2013). Cerebral blood flow and cerebrovascular reactivity at rest and during sub-maximal exercise: Effect of age and 12-week exercise training. *Age*, *35*(3), 905. https://doi.org/10.1007/S11357-012-9414-X

Papassin, J., Heck, O., Condamine, E., Pietras, J., Detante, O., & Krainik, A. (2021). Impaired cerebrovascular reactivity is associated with recurrent stroke in patients with severe intracranial arterial stenosis: A CO2 BOLD fMRI study. *Journal of Neuroradiology*, *48*(5), 339–345. https://doi.org/10.1016/J.NEURAD.2020.04.005

Paszke, A., Gross, S., Massa, F., Lerer, A., Bradbury, J., Chanan, G., Killeen, T., Lin, Z., Gimelshein, N., Antiga, L., Desmaison, A., Köpf, A., Yang, E., DeVito, Z., Raison, M., Tejani, A., Chilamkurthy, S., Steiner, B., Fang, L., … Chintala, S. (2019). PyTorch: An Imperative Style, High-Performance Deep Learning Library. *Advances in Neural Information Processing Systems*, *32*. https://arxiv.org/abs/1912.01703v1

Peirce, J. W. (2007). PsychoPy—Psychophysics software in Python. *Journal of Neuroscience Methods*, *162*(1–2), 8–13. https://doi.org/10.1016/J.JNEUMETH.2006.11.017

Peng, S. L., Chen, X., Li, Y., Rodrigue, K. M., Park, D. C., & Lu, H. (2018). Age-related changes in cerebrovascular reactivity and their relationship to cognition: A four-year longitudinal study. *NeuroImage*, *174*, 257–262. https://doi.org/10.1016/J.NEUROIMAGE.2018.03.033

Pinto, J., Bright, M. G., Bulte, D. P., & Figueiredo, P. (2021). Cerebrovascular Reactivity Mapping Without Gas Challenges: A Methodological Guide. *Frontiers in Physiology*, *11*, 1711. https://doi.org/10.3389/FPHYS.2020.608475/BIBTEX

Reddy, N. A., Zvolanek, K. M., Moia, S., Caballero-Gaudes, C., & Bright, M. G. (2024). Denoising task-correlated head motion from motor-task fMRI data with multi-echo ICA. *Imaging Neuroscience*, *2*, 1–30. https://doi.org/10.1162/IMAG_A_00057

Reybrouck, T., Mertens, L., Schulze-Neick, I., Austenat, I., Eyskens, B., Dumoulin, M., & Gewillig, M. (1998). Ventilatory inefficiency for carbon dioxide during exercise in patients with pulmonary hypertension. *Clinical Physiology*, *18*(4), 337–344. https://doi.org/10.1046/J.1365-2281.1998.00109.X

Schlund, M. W., Cataldo, M. F., Siegle, G. J., Ladouceur, C. D., Silk, J. S., Forbes, E. E., McFarland, A., Iyengar, S., Dahl, R. E., & Ryan, N. D. (2011). Pediatric functional magnetic

resonance neuroimaging: tactics for encouraging task compliance. *Behavioral and Brain Functions*, *7*, 10. https://doi.org/10.1186/1744-9081-7-10

Siegel, J. S., Snyder, A. Z., Ramsey, L., Shulman, G. L., & Corbetta, M. (2016). The effects of hemodynamic lag on functional connectivity and behavior after stroke. *Journal of Cerebral Blood Flow & Metabolism*, *36*(12), 2162. https://doi.org/10.1177/0271678X15614846

Slessarev, M., Han, J., Mardimae, A., Prisman, E., Preiss, D., Volgyesi, G., Ansel, C., Duffin, J., & Fisher, J. A. (2007). Prospective targeting and control of end-tidal CO2 and O2 concentrations. *The Journal of Physiology*, *581*(3), 1207–1219. https://doi.org/10.1113/JPHYSIOL.2007.129395

Sobczyk, O., Sam, K., Mandell, D. M., Crawley, A. P., Venkatraghavan, L., McKetton, L., Poublanc, J., Duffin, J., Fisher, J. A., & Mikulis, D. J. (2020). Cerebrovascular Reactivity Assays Collateral Function in Carotid Stenosis. *Frontiers in Physiology*, *11*, 569390. https://doi.org/10.3389/FPHYS.2020.01031/BIBTEX

Sobczyk, O., Sayin, E. S., Sam, K., Poublanc, J., Duffin, J., Fisher, J. A., & Mikulis, D. J. (2021). The Reproducibility of Cerebrovascular Reactivity Across MRI Scanners. *Frontiers in Physiology*, *12*, 668662. https://doi.org/10.3389/FPHYS.2021.668662/BIBTEX

Spano, V. R., Mandell, D. M., Poublanc, J., Sam, K., Battisti-Charbonney, A., Pucci, O., Han, J. S., Crawley, A. P., Fisher, J. A., & Mikulis, D. J. (2013). CO2 Blood Oxygen Level–dependent MR Mapping of Cerebrovascular Reserve in a Clinical Population: Safety, Tolerability, and Technical Feasibility. *https://Doi.Org/10.1148/Radiol.12112795*, *266*(2), 592–598. https://doi.org/10.1148/RADIOL.12112795

Stickland, R. C., Zvolanek, K. M., Moia, S., Ayyagari, A., Caballero-Gaudes, C., & Bright, M. G. (2021). A practical modification to a resting state fMRI protocol for improved characterization of cerebrovascular function. *NeuroImage*, *239*, 118306. https://doi.org/10.1016/J.NEUROIMAGE.2021.118306

Tancredi, F. B., & Hoge, R. D. (2013). Comparison of cerebral vascular reactivity measures obtained using breath-holding and CO 2 inhalation. *Journal of Cerebral Blood Flow and Metabolism*, *33*(7), 1066–1074. https://doi.org/10.1038/JCBFM.2013.48/ASSET/IMAGES/LARGE/10.1038_JCBFM.2013.48-FIG7.JPEG

Teopompi, E., Tzani, P., Aiello, M., Ramponi, S., Visca, D., Gioia, M. R., Marangio, E., Serra, W., & Chetta, A. (2013). Ventilatory Response to Carbon Dioxide Output in Patients with Chronic Heart Failure and in Patients with Chronic Obstructive Pulmonary Disease with

Comparable Exercise Capacity. *Respiratory Care*, *59*(7), 1034–1041. https://doi.org/10.4187/RESPCARE.02629

Thrippleton, M. J., Shi, Y., Blair, G., Hamilton, I., Waiter, G., Schwarzbauer, C., Pernet, C., Andrews, P. J. D., Marshall, I., Doubal, F., & Wardlaw, J. M. (2018). Cerebrovascular reactivity measurement in cerebral small vessel disease: Rationale and reproducibility of a protocol for MRI acquisition and image processing. *International Journal of Stroke*, *13*(2), 195–206. https://doi.org/10.1177/1747493017730740/ASSET/IMAGES/LARGE/10.1177_1747493017730740-FIG4.JPEG

Tisdall, M. D., Reuter, M., Qureshi, A., Buckner, R. L., Fischl, B., & van der Kouwe, A. J. W. (2016). Prospective motion correction with volumetric navigators (vNavs) reduces the bias and variance in brain morphometry induced by subject motion. *NeuroImage*, *127*, 11–22. https://doi.org/10.1016/J.NEUROIMAGE.2015.11.054

Wise, R. G., Pattinson, K. T. S., Bulte, D. P., Chiarelli, P. A., Mayhew, S. D., Balanos, G. M., O'Connor, D. F., Pragnell, T. R., Robbins, P. A., Tracey, I., & Jezzard, P. (2007). Dynamic forcing of end-tidal carbon dioxide and oxygen applied to functional magnetic resonance imaging. *Journal of Cerebral Blood Flow and Metabolism*, *27*(8), 1521–1532. https://doi.org/10.1038/SJ.JCBFM.9600465/ASSET/IMAGES/LARGE/10.1038_SJ.JCBFM.9600465-FIG4.JPEG

Yezhuvath, U. S., Uh, J., Cheng, Y., Martin-Cook, K., Weiner, M., Diaz-Arrastia, R., van Osch, M., & Lu, H. (2012). Forebrain-dominant deficit in cerebrovascular reactivity in Alzheimer's disease. *Neurobiology of Aging*, *33*(1), 75–82. https://doi.org/10.1016/J.NEUROBIOLAGING.2010.02.005

Zvolanek, K. M., Moia, S., Dean, J. N., Stickland, R. C., Caballero-Gaudes, C., & Bright, M. G. (2023). Comparing end-tidal CO2, respiration volume per time (RVT), and average gray matter signal for mapping cerebrovascular reactivity amplitude and delay with breath-hold task BOLD fMRI. *NeuroImage*, *272*, 120038. https://doi.org/10.1016/J.NEUROIMAGE.2023.120038